



ENGLISH LANGUAGE
FACULTY OF ENGINEERING

Final degree project:

**ALUMINIUM METAL MATRIX
COMPOSITE SINTERING WITH
ELECTROLESS METALLIZED
COMPONENTS**

Course 2018/2019

Author: Xabier Sandua Fernández

Tutors: Assoc. Prof. Dr. V. Kamburov

Assist. Prof. Dr. R. Dimitrova

20/05/2019



Deadline:

Dean:

Name: **Prof. Dr. T. Tashev**

FINAL YEAR PROJECT ASSIGNMENT

BEng course

1. Student's name: **Xabier Sandua Fernández** Faculty No: **223218007**

2. Project title: ALUMINIUM METAL MATRIX COMPOSITE SINTERING WITH ELECTROLESS METALIZED COMPONENTS

3. Basic project specifications:
Preparation and characterization of Aluminium Metal Matrix Composite (AlMMC) with electroless metalized reinforcing components. The metal matrix is aluminium alloy (AlSi9Cu3) turnings preliminary Ni-P and Ni-Cu-P coated at the same time as the reinforcing phase thereafter mixed and sintered together.

4. Contents:
 - a) Introduction
 - b) State-of-the-Art and trends Sintered P/M Aluminium Composites Technology
 - c) Formulation of design structure
 - d) Basic theory, analysis, synthesis, hardware and/or software development, design, block diagrams, justifications
 - e) Experiments and analysis
 - f) Conclusions

Project supervisors:

Deputy Dean:

Name: **Assoc. Prof. Dr. V. Kamburov**

Name: **Assoc. Prof. Dr. K. Dishlieva**

Assist. Prof. Dr. R. Dimitrova

ACKNOWLEDGEMENTS

To the Technical University of Sofia for allow me to study my final semester and to do my final degree project with them. With more accurately, to Prof. Dr. V. Kamburov, my tutor in this project and the one who make this project possible.

To the Public University of Navarre and all the professors who introduce me to this wonderful world of materials and they made this topic not only a subject for me but a hobby.

To my friends who made this stage of my life a more manageable time.

To my parents and to my brother Iñaki, who always is there to help me.

To Navarre for being so beautiful.

Index

ACKNOWLEDGEMENTS	3
ABSTRACT	5
STATE OF ART	6
<i>Introduction</i>	6
<i>Applications</i>	7
<i>Sintering process</i>	7
<i>Sintering process for Al composites</i>	8
<i>Sintering process for Al composites with SiC</i>	9
<i>Sintering process for Al composites with carbon nanotubes</i>	9
<i>Technology parameters</i>	10
<i>Metallic coating and Reinforcing materials</i>	12
<i>Effects of electroless Ni plating</i>	14
<i>Mechanical and physical properties</i>	16
<i>Al powder composites</i>	16
<i>Al powder composites sintered with SiC</i>	20
<i>Al powder composites sintered with carbon nanotubes</i>	24
<i>Future trends</i>	26
MATERIALS AND METHODS	28
<i>Electroless Ni-Cu-P of the components</i>	28
<i>Sintering of Aluminium Metal Matrix Composites</i>	31
<i>Dimensions of the sample</i>	34
<i>Tests procedure</i>	35
RESULTS	37
<i>Morphology and Structure of the AlMM Composites</i>	37
<i>Hardness of the AlMM Composites</i>	40
<i>Tribological properties of the AlMM Composites</i>	47
CONCLUSIONS	56
BIBLIOGRAPHY	57

ABSTRACT

This project will show the preparation and characterization of Aluminium Metal Matrix Composite (AlMMC) with electroless metallized reinforcing components. The metal matrix is aluminium alloy (AlSi9Cu3) turnings preliminary Ni-P and Ni-Cu-P coated at the same time as the reinforcing phase thereafter mixed and sintered together.

Different types of non-metallic reinforcement and un-reinforcement phases are used to create the sintered composites with aluminium powder, silicon carbide microparticles and carbon nanotubes (CNTs). A comparative analysis of the morphology, hardness and the elemental composition of the obtained composite materials were presented; also tribological research was performed.

STATE OF ART

Introduction

The increasing interest in light-weight materials show us the need for cost-effective processing, and they have combined to create a significant opportunity for aluminium powder metallurgy. This combination allow us the improvement of mechanical and even physical properties of so many substances. Powder Aluminium Composite is a great example of it, especially in the automotive area, its principal application.

It was originally produce by E. J. Hall in 1920. This American scientist used a stamp mill in order to create a powder of droplets and then he used a ball mill to transform them into flakes.

Nowadays, in order to produce this material, Powder Metallurgy Manufacturing Technique (P/M) is used, like sintering. A product example of this sintering is the one shown in Figure 1. The cost is quite competitive and it is consider a green manufacturing and energy efficient manufacturing technique if it is compared with casting. Besides, the products of the powder metallurgy are greatly advantageous over die castings and wrought products, in the fact that precise parts having near net shape and free of defects can be produced by a simple process.

The compositions of such a sintered aluminium alloy are usually similar to or belong to 2000 series or 6000 series of AA standard, which are heat treatable and hence can exhibit a high strength level.

An alternative to conventional alloys are metal matrix composites (MMCs), which have a high specific modulus, good wear resistance and a tailorable coefficient of thermal expansion. A major drawback to these MMCs is high cost. The reasons are twofold. First, the material itself is expensive because specially synthesised pre-alloyed powders are usually required and many processing steps are needed. The powders are typically cold pressed, then hot pressed or sintered and extruded. Canning and vacuum degassing are common. The second reason that these alloys are expensive is due to the high costs of secondary processing. They are not produced to near net shape and therefore require extensive forging or machining, which can be particularly problematical because of the ceramic component. Spray forming overcomes some of these problems by the direct formation of a near net shape billet. However, shapes are limited and processing is difficult.



Figure 1: Aluminium Sintered Powder

Applications

This material is used for wide range of industrial applications due to its exceptional properties. The major applications are located in aerospace, military and car industries, where they are used in cam bearing caps generally. This has been in service in the USA with Ford, DaimlerChrysler and General Motors since the early 1990s, without a failure. Potential automotive applications include connecting rods and oil pump gerotors in automatic transmissions where the sintered aluminium part will replace a sintered steel component. The major weight saving comes not from the direct material substitution, which is small for small parts, but through the potential for redesign. In gerotors, the major weight saving comes about by substitution of a cast iron housing with an aluminium die casting. However, a steel gear set inside an aluminium housing increases noise and vibration and decreases efficiency because of the mismatch between the coefficient of thermal expansion of the aluminium and the steel [1, 8].

An aluminium gear therefore facilitates the use of an aluminium housing. Connecting rods in North American passenger vehicles are currently made via powder forging using an Fe-Cu-C alloy. Because this is a reciprocating part, the inertial loads on other engine components are significant. Substitution of steel by aluminium will allow resizing of the crank shaft and ancillary equipment for substantial weight savings. In non-automotive applications, aluminium P/M parts may replace small aluminium die castings where the better material utilisation and closer tolerances of the P/M process are advantageous. Possible applications include pistons and coupling [8].

Low density and high toughness properties make this material an excellent option in order to work at high temperatures also, due to its high potential.

Because of their high corrosion and creep resistance, they are used in corrosive environments such as oil and gas wells, chemical process industry, marine environments, as automotive pistons, turbochargers, valves, aircraft fasteners, dental drills, forging dies, bearings, tubing, casting moulds for aluminium and glass, and heating elements for appliances [4].

There is significant industrial potential for aluminium alloys fabricated via net shape P/M techniques using inexpensive, elemental powder blends. In particular, the automotive industry demands both low weight and low cost materials in order to reduce fuel emissions and improve fuel economy at affordable prices. Additional potential markets for Al P/M parts include hand tools, where moving parts against gravity represents a challenge; and office machinery, where reciprocating forces are important. However, the properties of conventional, press-and-sinter aluminium P/M alloys are generally inadequate for many potential applications in these industry sectors [8].

Sintering process

Sintering is the process in charge of compacting the powder material and forming, with a certain die, a solid mass by the use of heat or pressure and without reaching the liquefaction, so it does not generate liquid from the solid.

Sintering can be considered a process of three stages: during the first stage powder particles remain discrete. In the second one, the structure recrystallizes and particles diffuse into each other. During the third stage, densification occurs at much lower rate.

Most of metals can be sintered but this process is applied especially to pure metals which have been produced in vacuum conditions.

This process has so many advantages like:

- Capable to produce components with high purity and with uniform porosity.
- Capable of controlling grain size during the input stages.
- No need of deformation in order to produce directional deformation of grains.
- Capable of achieving complex shapes and elements with high strength.

It also has some disadvantages:

- Not capable to create uniform sizes of an element.
- Production of nano- and micro-structures before sintering and then destroyed.

Sintering process for Al composites

The methods of compacting aluminium alloys powder are similar to the ones used for other powder materials. The only different is the outstanding compressibility of aluminium alloy powder, for example, air atomised aluminium powder can be compacted to 90% with pressures around the 165 MPa (while we need more less 700 MPa to reach the similar percent for iron powder). So smaller presses and fragile tools (because tool breakage is less likely) can be used with aluminium alloy powders [6].

Another important issue about aluminium sintering is the correct use of the lubricant. The lubricant has direct effect on the shape formation of the powder. In order to avoid any type of interaction with the powder, the lubricant should contain little portions of moisture and ash, and be inert to aluminium powder at delube temperature. Also depending in the aluminium alloy particle size, the use of the lubricant should be minimum [6].

This issues have been already studied for Al–Al₂O₃ composites and the effect of alumina particle size on the sintered density of the composite is depicted in Table 1. It indicates that by raising the particle size of alumina, there is a rise in the density; however, the relative density is reduced. This is because the density of alumina (3.97 g/cm³) is higher than aluminium (2.7 g/cm³). The lower relative density of the composite can be attributed to the reduction in compressibility when hard Al₂O₃ particles are added to aluminium powder. On the other hand, due to the vast difference in the melting point and compressive strength of the constituents, Al₂O₃ particles act as a barrier to the rearrangement, deformation and diffusion of the particles leading to higher porosity, irrespective to the sintering conditions. Raising the particle size of alumina from 3 to 12 µm leads to higher relative density. This suggests that a higher apparent and green density is achieved prior to sintering. However, further increase in size from 12 to 48 µm resulted in the lower relative density. It can be concluded that two concurrent consolidation mechanisms act between the ceramic phase and the metal one, in which lower alumina particle size leads to less porosity. Moreover, large alumina particles (48 µm) reduce the contact area between the aluminium (30 µm) particles, leading to higher porosity [1].

Particle size (μm)	Theoretical density (g/cm^3)	Sintered density (g/cm^3)	Relative density (%)
Pure aluminium	2.7	68	99.23
3	2.78	2.71	97.41
12	2.78	2.73	98.20
48	2.78	2.68	96.71

Table 1: effect of alumina particle size on the sintered density of the composite [1]

Sintering process for Al composites with SiC

Other studies shows the effect in sintering with SiC and aluminium composites. The following conclusions are achieved:

The production of SiC particle reinforced aluminium matrix composites in the form of net shape components and can be achieved successfully by the use of conventional powder metallurgical cold uniaxial pressing and sintering processing technology [17].

Sintering process for Al composites with carbon nanotubes

The procedure for fabricating Al sintered with carbon nanotubes (CNT) composites is shown in Figure 2. First, a precursor was prepared by the NSD (nanoscale dispersion) method with the goal of dispersing the CNTs in the aluminium powder. This precursor consisted of commercial gas atomized Al powder multi-walled carbon nanotubes (MWCNTs) and natural rubber (NR). The powder composition was adjusted in experiment for 5 vol% CNT–Al powder. The precursor was heat treated at 500 °C for 2 h in an argon atmosphere (1 l/min) to evaporate the NR. The obtained Al-CNT mixture powder was sintered in a carbon mould using a spark plasma sintering device manufactured by Sumitomo Coal Mining Co. Ltd. The sintering conditions were a maximum temperature of 600 °C, holding time of 20 min, heating rate of 40 °C/min, and pressure of 50 MPa. The sintered compact had a diameter of 15 mm and a length of 30 mm.

The sintered compact was extruded in a 60 °C conical die at 400 °C with a pressure of 500 kN. The extrusion velocity and the extrusion ratio were fixed at 2 mm/min and 20, respectively.

The macro-hardness of the extruded Al–CNT composite was evaluated using a Vickers hardness tester with a load of 200 g. The micro-hardness of the raw Al particle and extruded bulks were measured by a nano-indentor. The conditions for nano-indentation were a load of 0.4 g and a loading time of 10 s.

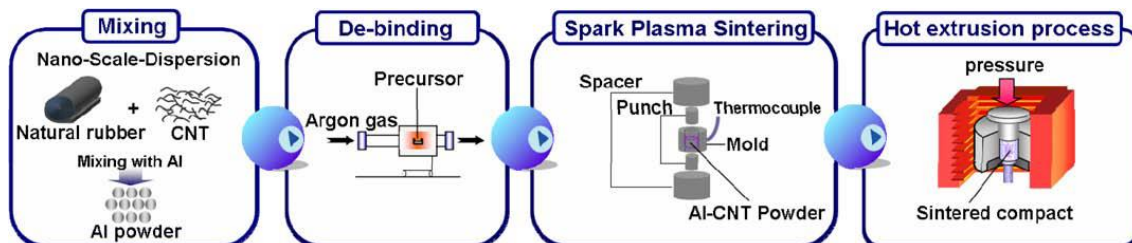


Figure 2: Sintering process for Al composites with carbon nanotubes [19]

The experiment obtain the properties shown in the Figure 3.

Table 1 – Some properties of the samples for every process.						
	Relative density	Oxygen content (wt.% ± 2%)	I_D/I_C	Vickers hardness (HV)	Nano-indentation (Hu, mN/ μm^2)	
Al powder	–	0.403	–	22	37	
Heat treated Al-CNT mixes powder	–	1.104	CNT:0.877 Al-CNT:0.831	–	–	
Sintered Al-CNT compact	96.1	0.798	0.858	–	–	
Extruded Al-CNT bulk	98	0.791	0.843	52	Pure Al:37 Al-CNT:40	

Figure 3: some properties of the samples of the process [19]

The SPS (spark plasma sintering) could fabricate Al-CNT with a relatively high density and degree of orientation for the CNTs. The CNTs were already well dispersed prior to this step because the NSD was used to produce a homogeneously mixed powder. Furthermore, grain growth in the matrix and damage to CNTs did not occur during the SPS, because of the pinning effect by the CNTs and oxides, and the rapid heating. A small quantity of carbide was generated during the SPS process and thereby affected a strong bonding between the Al matrix and CNTs. The subsequent hot extrusion process allowed further enhancements of density, dispersity, and CNT orientation. As a result, the slight addition of 5 vol% CNTs could remarkably elevate the strength to about thrice that of pure Al. The increase in the mechanical properties was attributed to particular strengthening by the CNTs, which strongly bonded with the matrix through the generated aluminium carbide phase [19].

Technology parameters

The quantitative formulation of sintering theory presents the equations linking some dimensional variables such as neck or pore radius or volume of a compact, with time and temperature prevailing during the process. All sintering equations contain a number of parameters such as diffusion coefficient, surface tension, particle size, initial pore volume, etc. One can divide these parameters into two classes:

- *Intrinsic*: these specify the intrinsic properties of the materials being sintered, such as surface tension, diffusion coefficient, vapour pressure, viscosity, etc. These properties change when the chemical composition, ambient atmosphere or temperature changes.
- *Extrinsic*: these depend on the geometrical or topological details of a system. These include parameters, as average particle size, particle or pore or grain shape and size distribution, etc.

These two classes of parameters are in some way or the other interdependent also. For example in the fabrication of fully dense Al_2O_3 , manipulation of chemistry of the system prevents the exaggerated grain growth, which in turn allows almost complete elimination of porosity.

This parameter's influence has been previously studied and this are the obtained conclusion in its parameter [16]:

- *Sintering atmosphere*: apart from adjusting the composition and impurity contents, sintering atmosphere also affects the sintering mechanisms. Gas transport rates are high and major changes are possible in pore structure, grain shape, impurity content, and sintering kinetics through sintering atmosphere. For example, several materials processed in a halide atmosphere show minimal shrinkage but accelerated coarsening due to enhanced vapour transport. Other microstructural changes are apparent in grain faceting, grain growth, surface area and pore size. A rationale is necessary to determine which atmospheres are most effective for impurity control, leading to the possible use of highly

active atmospheres. Pore mobility and pore size are affected by vapour transport, so there is an opportunity to independently influence the grain growth and pore mobility rates via temperature and atmosphere control.

Besides allowing composition adjustments, the sintering atmosphere affects the surface structure and in some instances gives a change in the vacancy population. This can be effective in metallic systems where oxidation and reduction cycles influence diffusion rates. Alternatively, vacuum sintering leads to preferential evaporation and loss of stoichiometry in surface regions.

- *Activate and liquid phase sintering*: the reactions of the systems to sintering depend on the relative solubilities of the species in one another, the relative surface energies and relative diffusion rates. Material transport occurs as a result of surface curvature and gradients in the concentrations of the atomic species. One major difficulty in understanding the exact means of operation of an additive is that so many alternative mechanisms for these process exist. Thus, for example, the additive can work as a second phase or as a solid solution:

As a second phase:

- Providing a high diffusivity path way
- Boundaries for diffusion across the boundary, which then acts to restrain grain boundary movement

As a solid solution:

- Enhancing diffusion coefficients for the controlling species in the lattice or parallel to the grain boundary by effecting the point defect concentrations in the boundary or lattice
- Slowing grain boundary movement by forming a segregated layer at the boundary which must then be pulled along by the boundary
- Altering the overall driving force for sintering by altering the ratio of grain boundary energy to free surface energy
- Slowing intrinsic grain boundary movement by reducing the diffusion coefficient for atom movement across the grain boundary, again by affecting the defect chemistry

- *Sintering of small size powders*: Novel sintered materials have been synthesised with mechanically alloyed powders. Metastable powders can be generated by intense attrition milling and these metastable structures can be preserved during sintering. It is desirable to have powders with reversible agglomeration and deagglomeration characteristics to adjust packing, handling and sintering behaviour. Superplastic forming is feasible with nanocrystalline materials and is preferable in some cases to pressure less sintering because of microstructure control. Research on grain growth during sintering for submicron size powders is still lacking. In the presence of liquid phase a still little information is available. The challenge here is to extend the knowledge available for large particles sintering to the small sized one.

The theories and models for sintering now available give reasonably good guidance for many of the operations and control variables such as size, temperature and rate effects.

Metallic coating and Reinforcing materials

Metallic coatings are applied in cases where the substrate is coated with a more noble metal, as with copper on steel. This type of protective coating is effective only when the coating is free from pores or damages. The defects in a metallic coating can cause severe damage to substrate via the formation of local cells.

Another variant of metallic coating is the coating of a substrate with a less noble material, as when steel is coated with zinc, or when aluminium is thermally sprayed on steel risers or offshore fixed structures. This type of coating is effective only when the corrosion product of the metal coating is able to restrict the corrosion process, and formation of aeration cells is stopped by the coating. The possibility of damage due to blistering and cathodic corrosion exists, and it must be addressed during the design stage, before selecting this type of metallic coating. The absorption and recombination of hydrogen is possible, and that can lead to blistering and cathodic corrosion. For both zinc and aluminium, additional protection can be provided by cathodic protection. The polarization properties and low protection current should be determined per each specific case. However, the protection potential must be limited toward the negative end. This limiting of the protection potential can, in turn, limit the formation of aluminates and zincates as corrosion products [14].

The major methods used for applying metallic coatings are:

- **Thermal spraying** of metal coatings, a gun is used that simultaneously melts and propels small droplets of metal onto the surface to be coated
- **Hot dipping** is carried out by immersing the metal on which the coating is to be applied, usually steel, in a bath of the molten metal that is to constitute the coating (Zn)
The coating consists mainly of two parts: an inner layer of Zn and Fe with contact with the base metal and an outer layer of Zn.
- **Diffusion** coatings of chromium, nickel, titanium, aluminum, and so on, can be prepared by immersing metal parts, under an inert atmosphere, in a bath of molten calcium containing some of the coating metal in solution.
- **Cementation** consists of tumbling the work in a mixture of metal powder and a flux at elevated temperatures, allowing the metal to diffuse into the base metal. Aluminum and zinc coatings can be prepared in this way.
- **Ion implantation** is a process of producing thin surface alloy coatings by bombarding the metal with ions *in vacuum*. Such coatings of, for example, Ti, B, Cr or Y have specialized applications for wear and high-temperature oxidation resistance.
- In **electroplating**, the substrate, or base metal is made the cathode in an aqueous electrolyte from which the coating is deposited, as can be seen in Figure 4.
Pure metals, alloys and mixed metals can be electro-deposited.

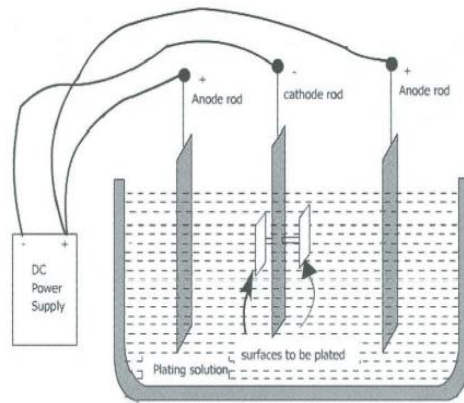


Figure 4: Electroplating

- Coatings are also produced by **electroless plating** – that is, by chemical reduction of metal-salt solutions, with the precipitated metal forming an adherent overlay on the base metal. As can be seen in Figure 5.

Better explain, electroless plating, also known as chemical or auto-catalytic plating, is a non-galvanic plating method that involves several simultaneous reactions in an aqueous solution, which occur without the use of external electrical power. It is mainly different from electroplating by not using external electrical power.

Here one of the main methods is **electroless nickel plating (EN)**, this is a reaction that deposits an even layer of nickel-phosphorus or nickel-boron alloy on the surface of a solid material, or substrate, like metal or plastic. The process involves dipping the substrate in a bath of plating solution, where a reducing agent, like hydrated sodium hypophosphite ($\text{NaPO}_2\text{H}_2 \cdot \text{H}_2\text{O}$), reacts with the material's ions to deposit the nickel alloy. The metallurgical properties of the alloy depend on the percentage of phosphorus, which can range from 2–5% (low phosphorus) to 11–14% (high phosphorus). Unlike electroplating, it is not necessary to pass an electric current through the plating solution to form a deposit. Electroless plating prevents corrosion and wear, and can be used to manufacture composite coatings by suspending powder in the bath. EN plating creates an even layer regardless of the geometry of the surface – in contrast to electroplating which suffers from flux-density issues as an electromagnetic field will vary due to the surface profile and result in uneven depositions. Depending on the catalyst, EN plating can be applied to non-conductive surfaces.

The process of EN is the following: before plating, the surface of the material is cleaned by applying a series of chemicals. Unwanted solids left on the surface cause poor plating. After applying each pretreatment chemical, the surface is rinsed two to three times with water to completely remove the chemicals. Removing oils is known as de-greasing, and removing scaling is known as acid cleaning.

The pretreatment required for the deposition of nickel and cobalt on a non-conductive surface usually consists of making the substrate hydrophilic, then activating the surface with a solution of a noble metal, like palladium chloride. Silver nitrate is used for activating ABS and other plastics. The composition of the electroless bath depends on the activator.

Activation is done with a weak acid etch, nickel strike, or a proprietary solution, if the substrate is non-metallic. After plating, an anti-oxidation or anti-tarnish chemical, such as trisodium phosphate or chromate, is applied, followed by rinsing with water to prevent

staining. The plated object is completely dried or baked to obtain the full hardness of the plating [15].

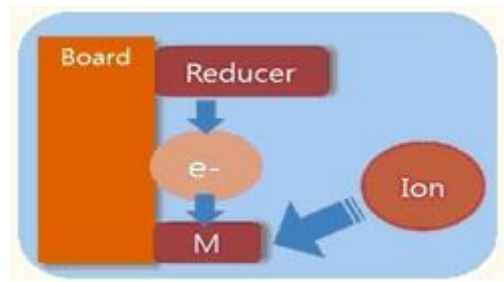


Figure 5: Electroless plating

Effects of electroless Ni plating

The plating of nickel in aluminium powder composites without electricity, have already been studied, in this case using a plasma reactor. With this mix a grey colour is obtained in the sample with the following size distribution [4]:

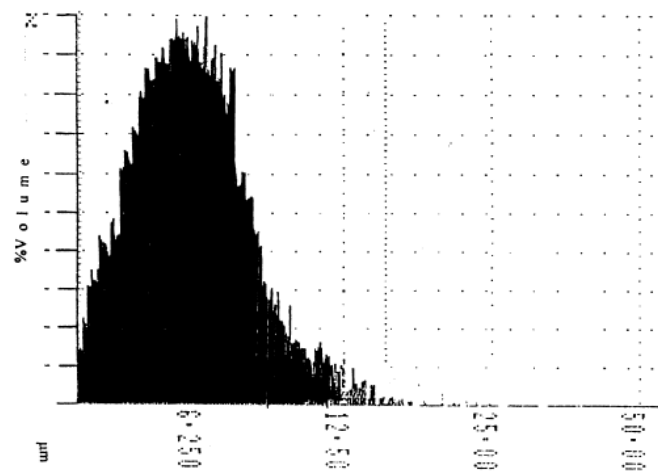


Figure 6: Particle size and distribution of nickel-plated aluminium powder [4]

Figure 6 shows that overall sizes were evenly distributed about 6 μm . The particle size numbers presented above are much finer than those reported in the literature, such as 15 μm for aluminium and 3–95 μm for nickel.

The initial aluminium powder particles were round-shaped whereas the nickel-plated aluminium powder particles had rounded, ligamental shapes, as shown in Figure 7 and 8, respectively. In the initial processing stage, aluminium vapor condensed on the chilled parts of the plasma reactor and, due to the surface energy, the aluminium condensate solidified to a spherical shape. In the subsequent plating process, the nickel deposited on the spherical aluminium particles as soon as the plating solution reached 90 $^{\circ}\text{C}$ while the pH was maintained at 10. Thus the time for deposition was limited. Nucleation and growth took place in the direction of the first starting nuclei and hence the plated particles usually assumed a ligamental shape [4].

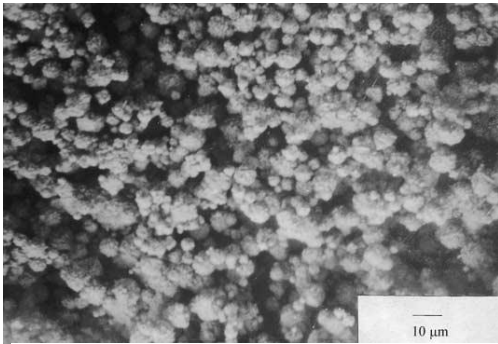


Figure 8: SEM micrograph of the Ni-plated aluminium powder [4]



Figure 7: SEM micrograph of aluminium powder produced in plasma reactor [4]

In order to improve the performance and the structural properties of the aluminium, the aluminium casting is electroplated with a heavy deposit of copper. After copper plating, the parts are then buffed again to further smooth out the surface. The final step is to activate the copper surface and electroplate with nickel chromium. Aluminium metal quickly forms an oxide which can weaken the plating adhesion. To prevent the oxide from forming, we use a zinc immersion film called a zincate prior to the nickel strike.

Another research shows the effect of electroless bath parameters and heat treatment on the properties of Ni-P and Ni-P-Cu composite coatings. The effect of pH, and the amount of Cu on the morphology, hardness, and the amount of alloying elements in Ni-P and Ni-P-Cu compositing coatings were investigated in this research. As well, the effect of heat treatment on the coating properties was analysed. The following results were obtained [22]:

1. In the coating with 1g/l Cu particle, the amount of P of the coating reduced from 7.06 to 4.12 by increasing the pH from 4.5 to 9. Therefore, increasing pH has reduced P due mainly to the fact that at higher pH, the reduction and precipitation of Ni is faster than P.
2. Cauliflowers morphology of the Ni-P coating was detected by SEM micrographs. And agglomeration was happening as the concentration of the particles increases from 1 to 7 g/l. The formation of lath features would affect the uniformity of the coating.
3. The growth rate of spheres was higher at higher pH due to higher rate of coating. The dominance of growth over nucleation at higher pH was explained to be the reason for this behaviour. More spheres were formed by increasing the pH from 4.5 to 7. While this trend was reversed by increasing the pH from 7 to 9.
4. Heat treatment for one hour at 400°C increased the hardness of the coatings substantially. This was due to the precipitation hardening effect of Ni₃P intermetallic phase. Moreover, the structure of mixed amorphous and crystalline nature changes to a fully crystalline one with the matrix of Ni and Ni₃P after performing the heat treatment process.
5. Although adding Cu particles reduced the hardness of Ni-P coating, within Ni-P-Cu composite coatings the hardness of Ni-P-Cu composite coating increased from 351.2 to 380.7 by increasing the Cu particles from 1 to 7 gr/lit. In fact, the higher the amount of particles in the coating, the higher would be the hardness values. The amount P was explained as the main reason for this increment.
6. Hardness of the composite coating increased with increasing the pH due to the fact that reducing P of the coating changes its structure from amorphous to crystalline. Though, the hardness at the pH of 9 was reduced as the result of alkaline nature of the bath.

Mechanical and physical properties

Al powder composites

Sintered aluminium powder alloys have properties quite different from those of material fabricated by conventional techniques. The oxide that forms immediately on the surface of aluminium is not reduced back to metal during sintering and the resulting powder product contains a substantial amount of oxide. This oxide prevents grain growth and movement of dislocations at the boundaries or through them and produces high strength, high creep resistance and insensitivity to high-temperature exposure [10].

The amount of oxide varies and its properties varies depending in the amount of naturally formed oxide. In order to increase the thickness of the oxide film a heating powder or addition of Al_2O_3 can be made. However, this processes does not increase the strength and only reduce the ductility of the material.

The oxide is present as finely dispersed particles, which interact with vacancies and dislocations and prevent their easy movement providing outstanding mechanical properties of the alloy. The oxide effect persists even above the melting point of aluminium [10]. When aluminium powder alloys undergo an asymmetric growth to reduction during the sintering because of the wettability issues caused by the inherent oxide films in the aluminium powder matrices, the micro-to-macro stresses experienced by the sintering body tend to develop defects in the sintering parts. Such defects certainly carry sufficient signatures on the severity, if there is any, when the powder parts go through expansion to reduction. The signatures are generally seen in aluminium powder parts as lateral bulging, formation of oval-top, formation of centre cracks, bending, delamination etc [12].

Sintered aluminium alloys has the following properties generally [11]:

- High strength
- High fatigue strength
- High creep resistance
- Excellent machinability
- Refractoriness (ability to retain the properties at elevated temperatures)
- Very good cryogenic properties
- Low coefficient of thermal expansion

If other characteristic are analysed [10]:

- Structure: the structure of SAP materials depends on the origin of the powder, but mainly on the fabrication technique and oxide content. The normal iron and silicon compounds present in aluminium fragment in powdering and become dispersed in the metal. They act as points of weakness and starting points for fracture, but the improvement of properties obtained by the use of aluminium 99.99% is limited.
- Density: the density is on the order of 900-1000 kg/m³, but when is compacted the values can reach 2710-2720 kg/m³, higher than that of the aluminium. Green and theoretical density increased with the increment of compaction pressure [9]. If heavy metals are added the density will raise also.
- Electric resistivity: if the oxide film is unbroken, as in the case after pressing and sintering only, resistivities as high as 1 Ωm have been measured; if, on the other hand, very high

temperature sintering (>800 K) or extrusion is used to break up the film, the resistivity drops by some 5-6 orders of magnitude.

- Grain strength: this depends on the contact area between the particles. The strength of the material after sintering is directly proportional and ductility is inversely proportional to the oxide content. Grain produce an increase in strength and ductility at high temperatures, but grain size of the product has little or no effect.
- Diffusivity: it has a high diffusivity. But elements, whose compounds tend to coalesce on high-temperature exposure, lose strength rapidly. Thus, duralumin, aluminium-copper and aluminium-zinc-magnesium alloys made by powder metallurgy have a strength at room temperature some 30-50% higher than the corresponding aluminium, but after 6 months exposure at 500-550 K have lost their extra strength at room temperature and at higher temperatures are weaker and less creep resistant. Age hardening of SAP alloys is not different from that of normal alloys.
- Texture: in extrusion tends to be of aluminium, but less pronounced, especially with fine size powders. High-speed extrusion produces a coarser structure but no substantial difference in properties.
- Recovery: is very similar to that of pure aluminium, but the mosaic structure is smaller, because dislocations tend to be pinned at oxide particles. Low-oxide materials (<3% Al₂O₃) recrystallise easily, but the recrystallisation temperature rises steeply with oxide content, so that above 5-7% Al₂O₃ recrystallisation, especially of extrusions, is very rare.
- Modulus of elasticity: increases with oxide content to reach values of the order of 77-80 GPa at 15-16% Al₂O₃, declining with temperature as the strength.
- Abrasion resistance: similar to the one of pure aluminium.
- Insensitivity to high temperatures: exposure for several years at temperatures up to 800 K produces practically no change in structure or properties, especially in the higher-oxide-content alloys.

The Table 2 show us the ultimate tensile strength and the yield strength of SAP as a function of temperature.

Property	% oxide	Temperature, K						
		170	300	500	600	700	800	900
UTS MPa	1	-	80-140	-	60-80	40-70	-	-
	3	-	150-220	-	-	60-80	-	-
	7	350	230-280	120-150	100-140	70-100	50-70	-
	12	400-500	320-380	180-220	150-190	100-140	60-90	-
	15	-	400-500	200-250	150-200	100-150	70-100	40
YS MPa	1	-	40-70	-	40-60	-	-	-
	3	-	100-140	-	-	-	-	-
	7	-	120-160	100-140	80-120	60-90	40-80	-
	12	250-300	180-240	140-180	110-150	80-120	60-90	-
	15	-	200-260	170-220	140-200	100-150	80-100	30

Table 2: mechanical properties of SAP as function of temperature [10]

But the most important properties are [10]:

- Low coefficient of thermal expansion: is lower than for pure aluminium and decreases almost linearly with increasing oxide content, to reach values of the order of $20 \times 10^{-6} / \text{K}$ for the 300-600 K range at 15% oxide. Thermal conductivity decreases by approximately 1% for every 1% of oxide present, but is higher in the direction of extrusion. Repeated pressing with intermediate vacuum annealing gives the maximum conductivity.
- High fatigue strength: is of the order of 60-70 MPa at 10^7 cycles and the decrease with temperature parallels that of the strength. Fatigue resistance is increased by some 10-20% by high hydrogen in solution but decreased clearly by notches and slow strain rates. Besides, it is higher in vacuum.
- High creep resistance: is extremely high and exceeds that of all aluminium alloys. Activation energy for creep of 6.5 eV has been reported. Impact strength rises with increasing temperature up to 800-850 K and then declines; shear strength behaves similarly.

The workability behaviour of powder metallurgy aluminium composites have been studied too. The upsetting tests on Al-4%TiC, Al-4%WC, Al-4%Fe₃C, and Al-4%Mo₂C cylindrical powder metallurgy preforms were carried out [3]. In this study strain ϵ_{err}^f and stress β^f formability are measured, that is, the ability of a given metal to undergo the plastic deformation without being damaged.

The Table 3 show the obtained results of the experiment.

Composition	Relative density	Aspect ratio	ϵ_{err}^f	β^f
Al-4%TiC	0.82	0.2	0.1506	3.4845
		0.4	0.1820	2.8096
		0.6	0.1698	2.0257
	0.86	0.2	0.1335	4.3333
		0.4	0.1462	3.5322
		0.6	0.1559	3.0762
Al-4%WC	0.82	0.2	0.1557	1.8606
		0.4	0.1882	1.8209
		0.6	0.1705	1.7242
	0.86	0.2	0.1132	2.5488
		0.4	0.1709	1.9264
		0.6	0.2753	1.1064
Al-4%Fe ₃ C	0.82	0.2	0.1321	3.0028
		0.4	0.1444	2.6134
		0.6	0.1569	2.4027
	0.86	0.2	0.1264	3.3642
		0.4	0.0901	4.5001
		0.6	0.1769	2.7961
Al-4%Mo ₂ C	0.82	0.2	0.2938	2.5641
		0.4	0.1789	2.6111
		0.6	0.2161	2.4735
	0.86	0.2	0.1260	3.5085
		0.4	0.1664	2.9745
		0.6	0.1706	2.8182

Table 3: workability of some aluminium composites [3]

Another different powder blends have been investigated in order to achieve a high wear resistance and strength, this is shown in Table 4.

Name	Base material [wt.%]						Reinforcing material vol.%
	Al	Si	Cu	Mg	Sn	Fe	
A	Bal.	14.8	2.50	0.58			-
B	Bal.	0.67	4.30	0.47		0.09	2 ZrSiO ₄ edged, <75 μm
C	Bal.	0.30	3.09	1.46	0.61	0.11	2 ZrSiO ₄ edged, <75 μm
D	Bal.	0.30	3.09	1.46	0.61	0.11	2 (ZrO ₂ + SiO ₂) spheric, 0-63 μm
E	Bal.	0.34	3.04	1.47	0.61	0.13	2 Al ₂ O ₃ edged, < 100μm

Table 4: types of samples of an experiment [18]

Obtaining the results shown in the Figure 9 regarding the press/sintering behaviour.

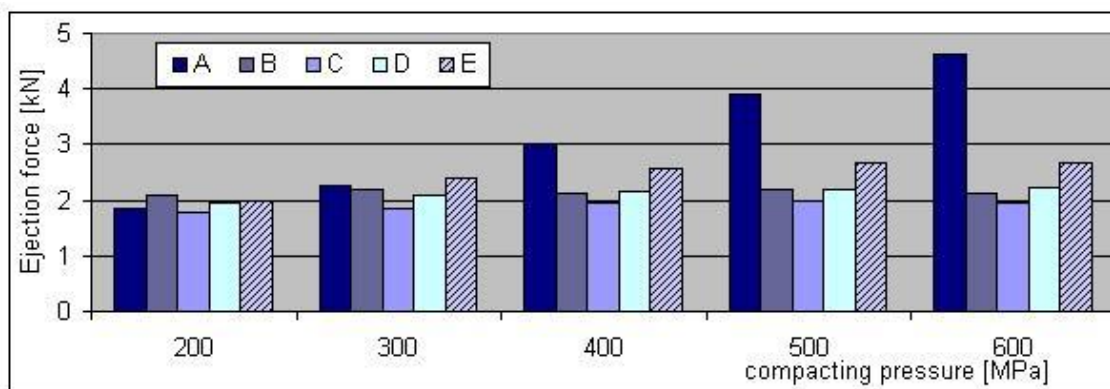


Figure 9: Ejection force of alloys vs the compacting pressure [18]

Where can be seen that the highest green densities are achieved by the powder blends C-E, taking into account that they are based in the same aluminium matrix.

Now, regarding the mechanical properties in artificially aged conditions are shown in Figures 10, 11 and 12.

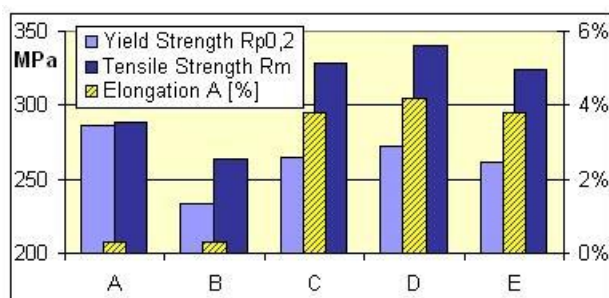


Figure 10: Tensile strength and elongation [18]

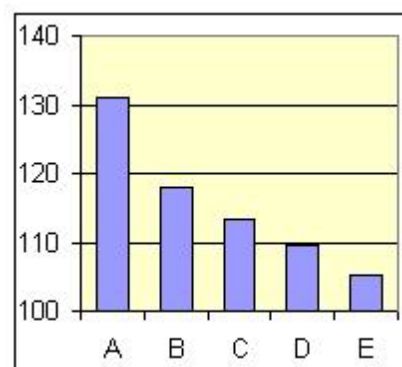


Figure 11: Brinell-Hardness [18]

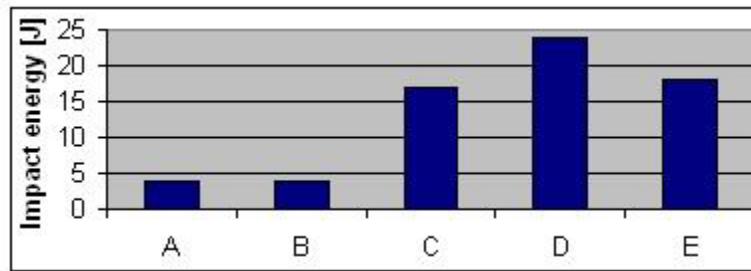


Figure 12: Impact energy [18]

In the Figure 10 and 11 can be seen the advantage that the alloys C-E have in elongation and in impact energy with respect the other ones. However A and B have higher hardness as can be seen in figure 11.

Finally the study also perform a tribological test, shown in Figure 13.

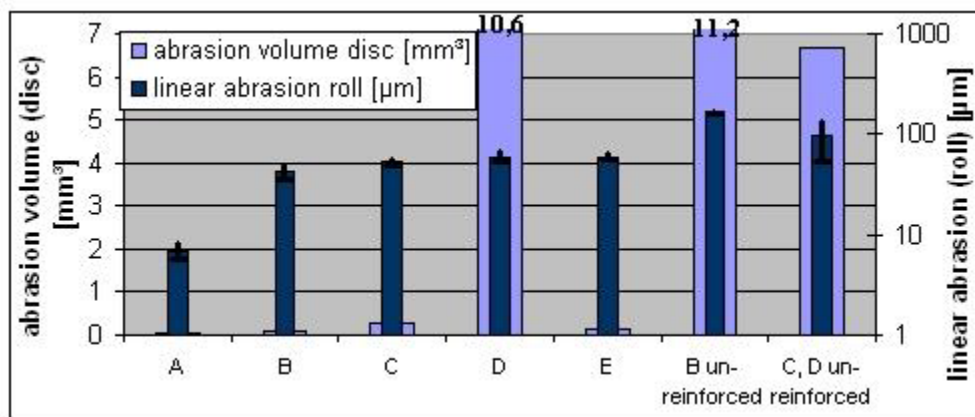


Figure 13: Linearly reciprocating tribometer test [18]

As can be seen in Figure 13, alloy A shows an excellent wear behaviour whereas the abrasion of the P/M aluminium discs and steel rolls are increased for samples B, C and E. All tests of alloy D had to be cancelled because of achieving the stop criterion. That is probably caused by the low interfacial bonding and fracture strength of the used spherical ceramic particles. The tests of unreinforced variants of alloys B and C/D had to be cut short too [18].

So the test surface has an important influence on the abrasion of wear partners, caused of a possible non uniform particle distribution.

The reinforcement of P/M aluminium alloys with small amounts of hard particles (2 volume %) leads to an significant increase of the wear resistance compared to the base alloy without a noticeable degradation of the mechanical properties.

Al powder composites sintered with SiC

In order to see the influence of SiC in Al powder composites an experiment has been made with the samples shown in Table 5.

Sample	Aluminium		Silicon carbide	
	Percentage(%)	Weight(gms)	Percentage(%)	Weight(gms)
A	100	7.15	0	0
B	90	6.44	10	0.8
C	80	5.71	20	1.7
D	70	5.0	30	2.6

Table 5: types of samples of another experiment [20]

Sample A:

- Vickers Hardness: (2.50 dia ball)
37.5 HBW - 62.5 Kgf Load
36.3 HBW - 62.5 Kgf Load
37.2 HBW - 62.5 Kgf Load
- The crush with 10 mm ball can be seen in Figure 14.

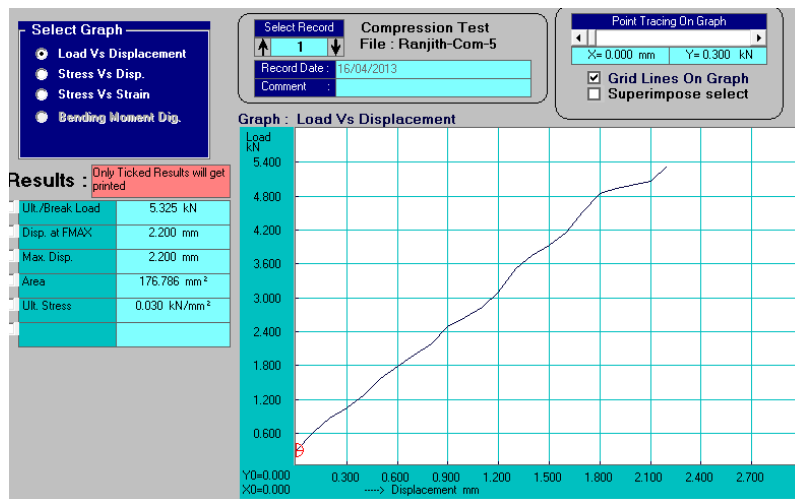


Figure 14: Load vs Displacement of sample A [20]

This graph show us that the sample A is quite brittle, that is, high stiffness.

- The microstructure can be seen in Figure 15.

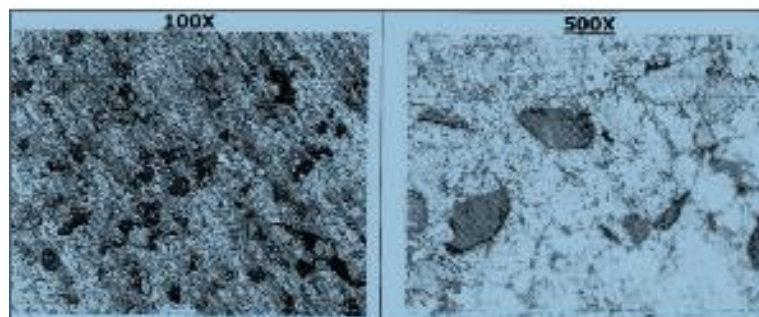


Figure 15: Microstructure of sample A [20]

The image shows compacted and sintered Aluminium powder metallurgical product. The photo micrograph shows some pores and good fusion aluminium powder. As the mix is with SiC

powders aluminium powder the matrix shows the uniform distribution of the SiC in aluminium matrix. The powder size of the Sic is seemed to be not of same sizes and some are larger.

Sample B:

- Vickers Hardness: (2.50mm dia ball)
 - 32.3 HBW - 62.5 Kgf Load
 - 31.8 HBW - 62.5 Kgf Load
 - 31.9 HBW - 62.5 Kgf Load
- The crush with 10 mm ball is shown in Figure 16.

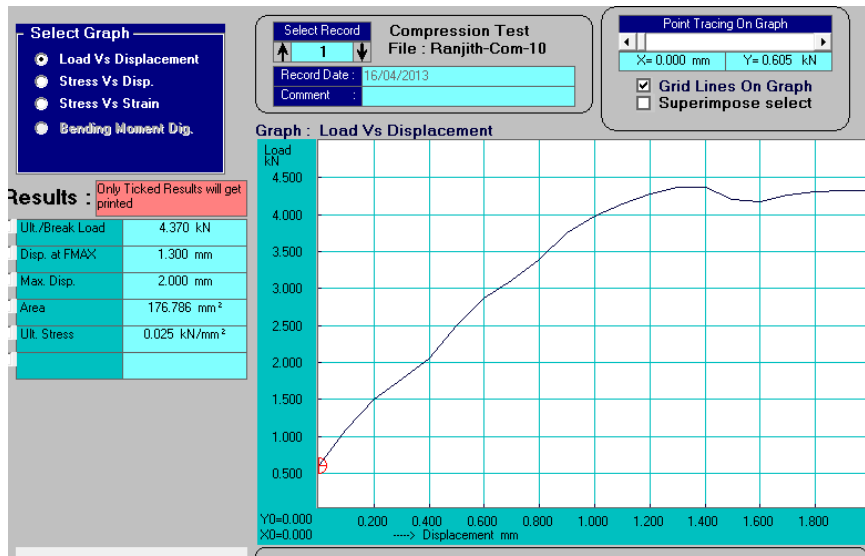


Figure 16: Load vs Displacement of sample B [20]

The sample B show us more ductility and less stiffness, due to the shape of the graph.

- The microstructure is shown in Figure 17.

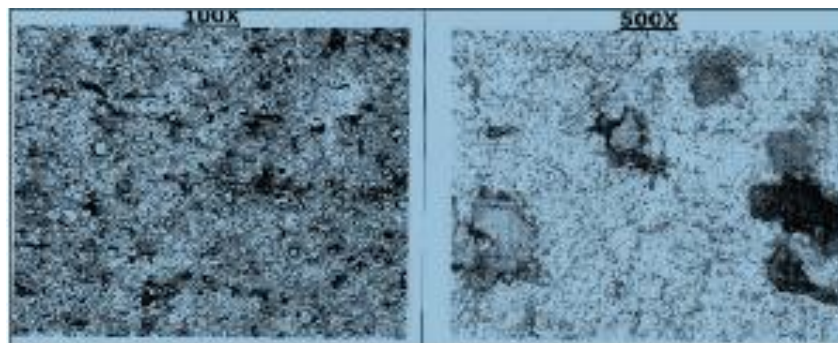


Figure 17: Microstructure of sample B [20]

The image shows compacted and sintered Aluminium powder metallurgical product. The photo micrograph shows some pores and good fusion aluminium powder. As the mix is with SiC powders aluminium powder the matrix shows the uniform distribution of the Sic in aluminium matrix. The powder size of the Sic is seemed to be not of same sizes and some are larger. As the percentage of the composite particles is higher the matrix is with more particles of SiC.

Sample C:

- Vickers Hardness: (2.50mm dia ball)
37.4 HBW - 62.5 Kgf Load
36.7 HBW - 62.5 Kgf Load
36.2 HBW - 62.5 Kgf Load
- The crush with 10 mm ball can be seen in Figure 18.

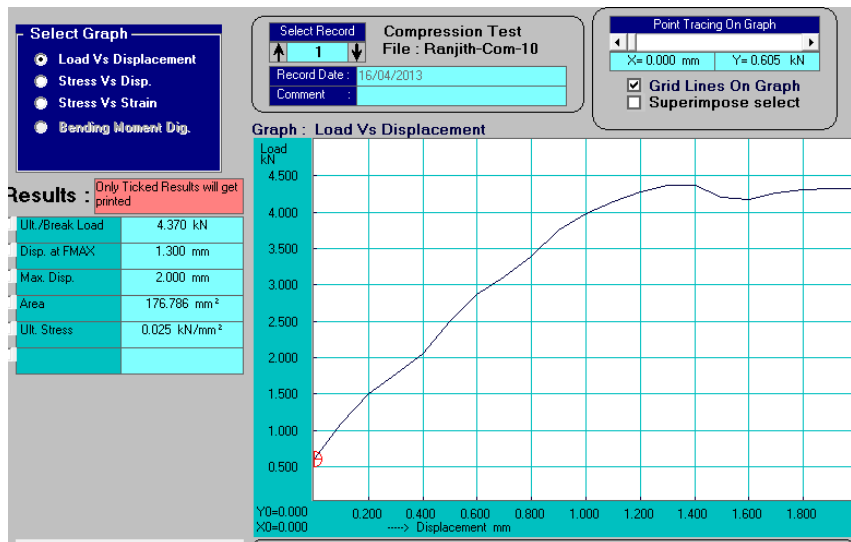


Figure 18: Load vs Displacement of sample C [20]

The sample C show us a high ductility and less stiffness. With this percentage of SiC it is obtained the lowest hardness.

- The microstructure can be seen in Figure 19.

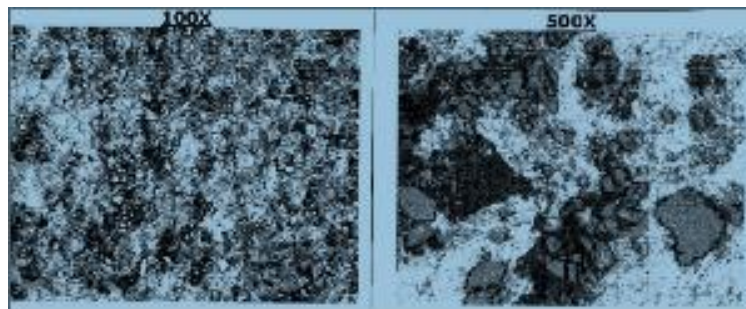


Figure 19: Microstructure of sample C [20]

The image shows compacted and sintered Aluminium powder metallurgical product. The photo micrograph shows some pores and good fusion aluminium powder. As the mix is with SiC powders aluminium powder the matrix shows the uniform distribution of the Sic in aluminium matrix. The powder size of the Sic is seemed to be not of same sizes and some are larger. As the percentage of the composite particles is higher the matrix is with more particles of SiC.

The behaviour to hardness will be the one in the Figure 20.

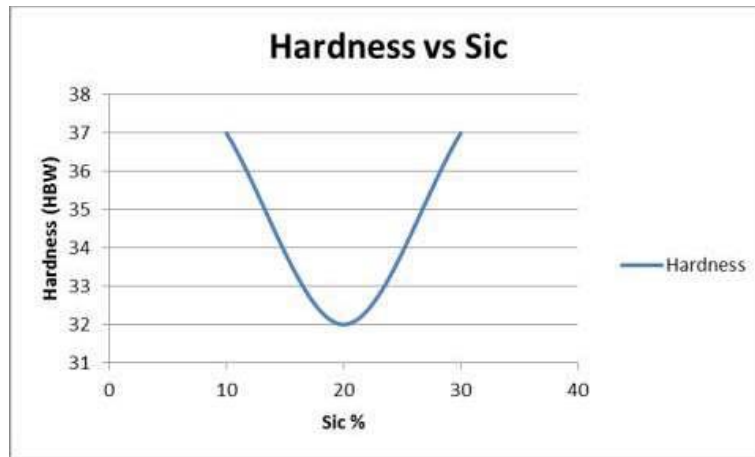


Figure 20: Behaviour of hardness with SiC amount [20]

The SiC particle penetration of the aluminium powder oxide layer, which occurs during composite powder pressing allows for subsequent aluminium transportation during the sintering process. If the distribution and incidence of the powder penetration is sufficient, the sintering response of the component should be adequate to allow near complete consolidation of the composite.

The size and size distribution of the aluminium powder affect strongly the sintering response of the green components and, therefore, also affect greatly the material characteristics of the sintered component. A narrow distribution of aluminium powder size and an absolute size similar to that of the SiC particles used should result in a composite, which is well sintered and does not exhibit particle clustering. Conversely, a wide distribution of aluminium powder will result in a material, which exhibits a sintered component microstructure containing undesirable small unsintered aluminium powders and particle clusters.

As the volume fraction of SiC drops, the interaction during pressing between the SiC and aluminium powder reduces. Therefore, in order to increase the incidence of interaction, the SiC particle size should be reduced. Consequently, the aluminium powder size must also be reduced to maintain the SiC particle size to aluminium powder size relationship. However, very low volume fractions of approximately 5% SiC or lower should be avoided since the incidence of interaction may not be sufficient to allow for complete sintering.

The use of die wall lubrication during compaction and ejection should be selected in preference to mixed in lubrication.

Due to the highlighted importance of powder and particle size and SiC volume fraction, it should be noted that as powder and particle size decrease, and volume fraction increases the compaction pressure required to achieve a specific green density increases. Therefore, the selection of a suitable compaction pressure must be based on these parameters for any given composite [17].

Al powder composites sintered with carbon nanotubes

Figure 21 shows the TEM micrograph of as-received carbon nanotubes. It is very evident that carbon nanotubes are tangled together; their diameters are between 20 and 40 nm and lengths range from hundreds of nanometres to micrometres. Most of them are not straight and possess some defects and localized kinks and bends. Moreover, some large black areas can also be seen. Energy dispersive X-ray (EDX) measurements indicate that the black areas consist of La and Ni. Considering the impurities affect significantly the dispersion of carbon nanotubes, the as-received carbon nanotubes were purified by the reflux in concentrated nitric acid to remove the impurities and reduce the aspect ratio of carbon nanotubes. It can be clearly seen from Figure 21 (b) that the

purified carbon nanotubes are uniformly dispersed, their surfaces are very clean. Meanwhile, the aspect ratio of carbon nanotubes is largely decrease, no other impurities particles are found during TEM observation [21].

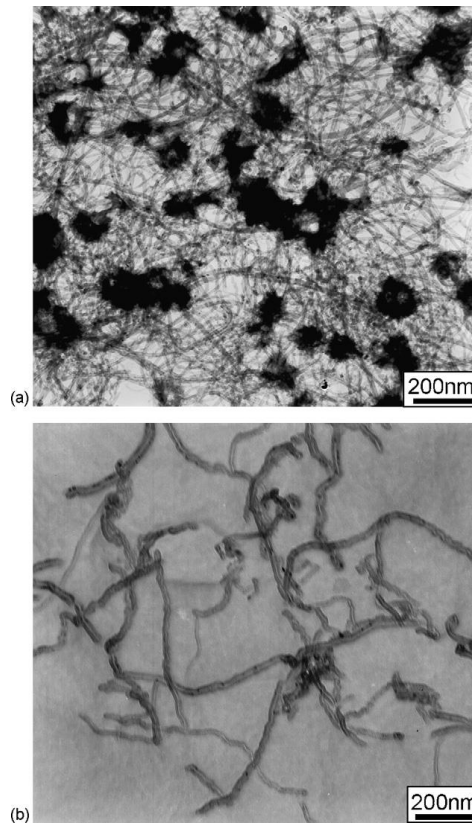


Figure 21: TEM images of CNTs, a) raw CNT b) purified CNT [21]

The effects of carbon nanotubes content on relative density and hardness are shown in Figure 22. It is evident that with small amount of carbon nanotubes addition, the relative density and hardness of the composites increase with increasing carbon nanotubes content, while large amount of carbon nanotubes reduce the relative density and hardness of the composites. This can be due to the fact that small amount of carbon nanotubes addition could fill up the micro voids resulting in increase of the density of CNT–2024Al composites (this experiment’s sample), however, large amount of carbon nanotubes are prone to tangle together in blended powders of 2024Al powders and carbon nanotubes. Carbon nanotubes conglomeration not only impedes the densification of the specimens, but also becomes the defect source. Hence, the relative density and hardness of the composites decreases.

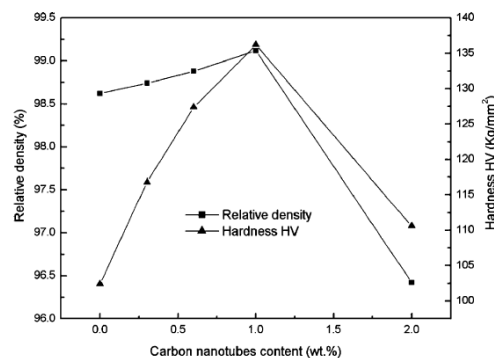


Figure 22: Relative density vs amount of CNT [21]

The tensile strength, Young's modulus and elongation of composites as function of carbon nanotubes content is shown in Figure 23. It can be seen that carbon nanotubes content affects elongation of composites. The tensile strength and Young's modulus firstly increases with increasing carbon nanotubes content when carbon nanotubes content is below 1.0 wt.%, but decreases obviously with increasing carbon nanotubes content. The tensile strength and Young's modulus reaches the maximum when carbon nanotubes content is 1.0 wt.%. The maxima of tensile strength and Young's modulus of the composite are 521.7 MPa and 102.2 GPa, respectively; those are enhanced 35.7% and 41.3% compared with the matrix material fabricated under the same process, respectively. The phenomena can be due to the factors that with the addition of very small amount of carbon nanotubes, carbon nanotubes are distributed uniformly in the composites leading to dispersion strengthening, and fill up the voids resulting in increase of the relative density of composites.

Meanwhile, the dispersing carbon nanotubes restrain the growth of Al grains during fabrication of the composites bringing on grain refinement strengthening. So the mechanical properties of composites increase with increasing carbon nanotubes content.

However, more quantity of carbon nanotubes impede the densification process resulting in the decrease of the relative density of composites, moreover the bonding between carbon nanotubes in the conglomeration is very weak, leading to the deterioration in mechanical properties. It is also very interest to note that the elongation of composites keeps almost invariable when carbon nanotubes content is below 1.0 wt.%. This can be owing to the fact that carbon nanotubes can increase the toughness of the composites by absorbing energy because of their highly flexible elastic behaviour during loading, which is markedly different from the traditional fibres or whiskers, but need to be verified [21].

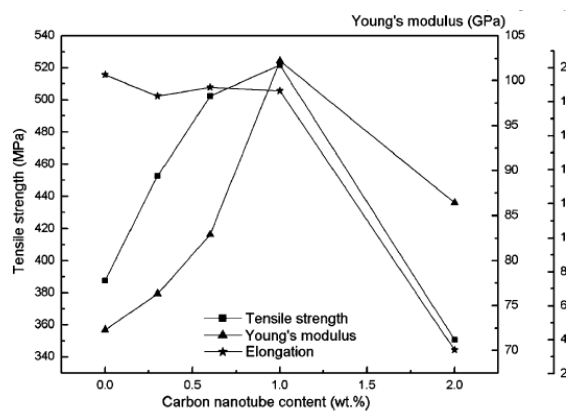


Figure 23: Tensile strength vs amount of CNT [21]

Future trends

Although aluminium powder is easily available, aluminium P/M unfortunately remains a minor participant in the overall aluminium powder market. Similar to the development of any other manufacturing industry, the future of aluminium P/M will largely depend on more value-added innovative designs and products and improved productivity. This will require relentless innovation in R and D. At present aluminium P/M parts are used primarily in low-stress applications where the combination of low-grade properties and net shape forming capability is required.

P/M has significant advantages over casting in composite design and fabrication. In addition to the usual tensile strength data, a significant improvement in the stiffness of aluminium P/M parts, for example >100 GPa, at a cost-effective approach will open new markets for aluminium P/M. Aluminium P/M composites thus still represent an important research direction. They are likely to find applications in advanced transmissions such as dual-clutch designs and continuously variable.

Fatigue is an important design consideration for P/M parts subject to dynamic stresses. In general, the fatigue strength of press and sinter aluminium P/M parts is about half that of wrought alloys of corresponding composition (ASM, 1998). While this is suitable for low-stress non-dynamic applications, much improved fatigue strengths are necessary in order for the aluminium P/M parts to penetrate into highly loaded applications in the drive train systems of automobiles. Because of the involvement of pores, the fatigue of a sintered aluminium alloy may differ appreciably from that of a cast or wrought alloy of similar composition. At present experimental data on the fatigue of sintered aluminium alloys are still very limited transmissions [6].

MATERIALS AND METHODS

In this section will be described the materials and methods used to produce the sintered aluminium metal matrix composite with electroless metallized components.

As the aluminium metal matrix, a cast aluminium alloy (EN AB-AlSi8Cu3) is used. This material has been made with a cross-section of 0.1 mm x 0.05 mm.

The mechanical properties of the basic aluminium alloy EN AB-46200 (DIN 226) are as follows:

- A Brinell Hardness of 82
- A yield strength of $R_p(0.2) = 130$ MPa
- A ultimate strength of $R_m = 210$ MPa

The physical properties are as follows:

- A density of 2.8 g/cm³
- A melting onset (solidus) at 540 °C
- A melting completion (liquidus) at 620 °C
- A electric conductivity between 13 - 17 MS/m
- A modulus of elasticity 7500 kg/mm²
- A thermal conductivity at 20 °C of 110 - 120 W/(m K)

Finally, some qualitative properties:

- Good strength at elevated temperatures (200 °C)
- Low general resistance to corrosion
- Excellent machinability
- Good castability
- Medium polishing
- Medium resistance to hot tearing
- Medium pressure tightness
- Good weldability
- Insufficient decorative anodising
- Medium protective anodising

The powder size of the components have to be taken into account too. The aluminium powder's size has a 100 µm max. It is stabilized with 2% fat and has a 90% in base substance.

The silicon carbide is 7 - 10 µm fraction and it is mixed with aluminium powder in a 1:1 ratio.

Finally, the carbon nanotubes (CNTs) had an average diameter of 10 - 40 nm and a length of 1 - 25 µm, a purity by weight 93 % and a specific surface area 150 - 250 m²/g.

Electroless Ni-Cu-P of the components

After an appropriate surface preparation a chemical nickel-copper coated has been applied to all the components for sintered composite material.

The solution for electroless ultrasonic treatment for realization of the Ni–Cu–P coating procedure contains, as follows:

- Nickel chloride ($NiCl_2 \cdot 6H_2O$) \rightarrow 25 – 40 g/l
- Copper sulphate ($NiSO_4 \cdot 6H_2O$) \rightarrow 10 – 25 g/l
- Ammonium citrate ($(NH_4)_2C_6H_6O_7 \cdot H_2O$) \rightarrow 50 – 80 g/l
- Sodium citrate ($Na_3C_6H_5O_7 \cdot 2H_2O$) \rightarrow 30 – 50 g/l
- Sodium hypophosphate ($NaH_2PO_2 \cdot H_2O$) \rightarrow 10 – 20 g/l

When we are dealing with CNTs, we have to prepare its surface so a surface cleaning is required. This is done with acetone (CH_3COCH_3). Also, a surface modification is carry out with the following stages: oxidization in concentrated nitric acid (HNO_3); sensibilization and chemical activation in solution, containing $PdCl_2$ and $SnCl_2$ dissolved in 3 M hydrochloric acid (HCl). The result from the fibre modification and the removal of the oxide layer from the aluminium powder is the creation of a low pH at the dispersion phase surface and accordingly the reduction of the total pH of the metallization suspension.

After electromagnetic stirring the suspension for the plating, along with the activated aluminium powder / SiC / CNTs has a pH value of 5.

The suspension is alkalinized with ammonia to pH 9-10 under ultrasonic treatment. The alkalises of the suspension with ammonia results in a gradual initiation of an exothermic reaction at room temperature resulting in an intense release of hydrogen in the form of bubbles. This reaction is maintained by the treatment in an ultrasonic bath without the need for further heating of the suspension.

The degreased aluminium turnings ($AlSi8Cu3$) are added to the carbon nanotubes or aluminium powder suspension with a started release of hydrogen, and is waited until the ultrasonic bath reaction is complete. The dense suspension containing the aluminium turnings is transferred from the bath for ultrasonic treatment to electromagnetic stirring.

The suspension is diluted with a new solution and stirred intensive at 1800 rpm. The reaction may be accelerated and the metallization re-started by further heating to 70-800 °C. The colour of the suspension with light aluminium alloy turns gradually darkens. After the completion of the metallization, the suspension is coloured in black due to the deposited nickel-copper-phosphor coating and the surface of the aluminium turnings.

After the completion of the co-nickel-copper metallization of the disperse phase and the aluminium turnings, they are filtered through a filter paper ("blue strip"). After an air drying, the metallized components of the composite material are pulverized to a powder state.

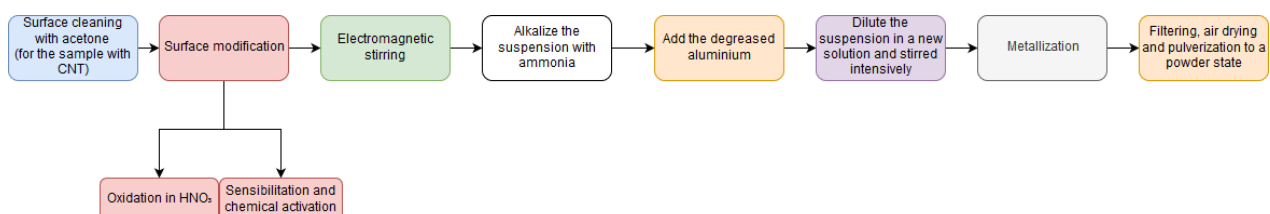


Figure 24: Block diagram of the electroless plating

Once we have done this is necessary to carry out a SEM analysis. This type of analysis employ electron beams in order to get information from a sample at the nanoscale. The sample emits secondary electrons that are then detected. The number of electrons depends on the variation of the sample surface. So the beam is scanned and detecting the variation of the number of emitted electrons we can reconstitute the surface topography.

Every atom has a unique number of electrons that reside under normal conditions in specific positions. These positions belong to certain shells, which have different, discrete energies.

The generation of the X-rays in a SEM is a two-step process called EDX. In the first step, the electron beam hits the sample and transfers part of its energy to the atoms of the sample. This energy can be used by the electrons of the atoms to “jump” to an energy shell with higher energy or be knocked-off from the atom. If such a transition occurs, the electron leaves behind a hole. Holes have a positive charge and, in the second step of the process, attract the negatively-charged electrons from higher-energy shells. When an electron from such a higher-energy shell fills the hole of the lower-energy shell, the energy difference of this transition can be released in the form of an X-ray.

This X-ray has energy which is characteristic of the energy difference between these two shells. It depends on the atomic number, which is a unique property of every element. In this way, X-rays are a “*fingerprint*” of each element and can be used to identify the type of elements that exist in a sample.

From the Energy Dispersive X-ray EDX analysis (EDX) shown in Figure 25 it can be seen that when co-metallization with the described ultrasonic treatment solution, the nickel and copper peaks are almost equal, which implies the coating of all sintering components with a copper-nickel-based alloy.

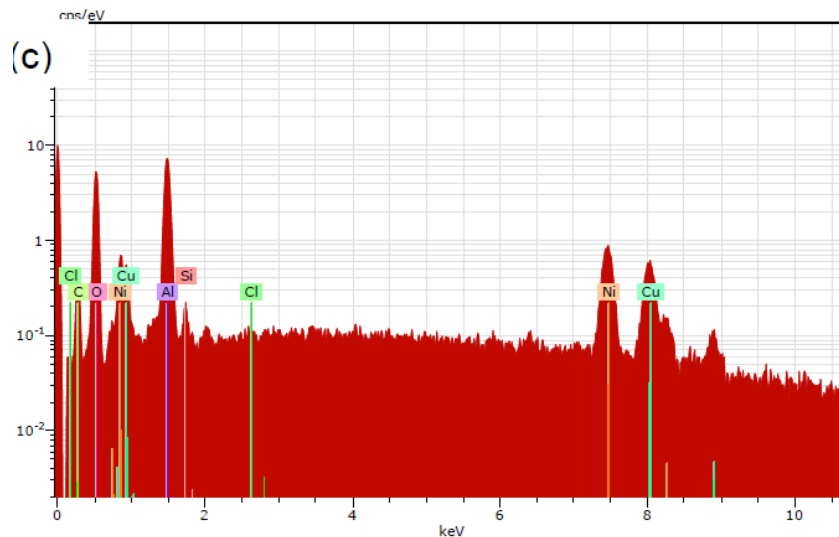


Figure 25: EDX spectrum

Then, the scanning electron microscopy show us the picture of our sample, this can be seen in Figure 26.

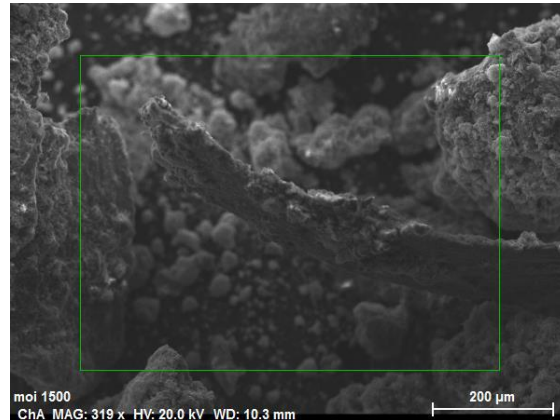


Figure 26: SEM image

Also an EDX mapping of the sample has been obtained and it is shown in Figure 27.

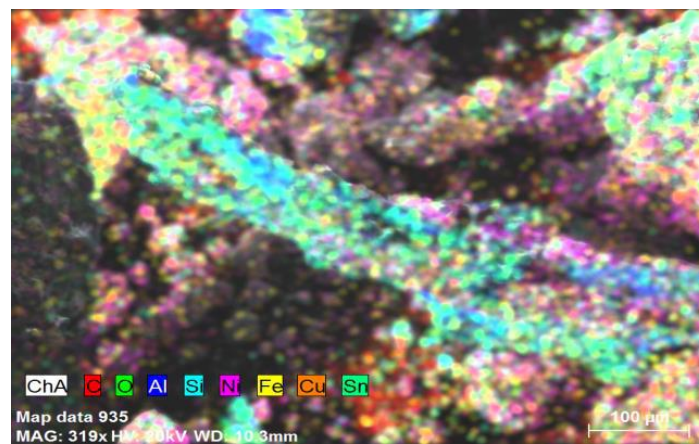


Figure 27: EDX mapping

This Figure 27 show us the particle distribution of our sample separating the different components with different colours.

Sintering of Aluminium Metal Matrix Composites

In order to carry out the experiments of hardness and wear resistance is necessary the production of the sample. The co-metallized dispersed phase and aluminium alloy turnings involves several major steps:

- Blending: is the process of solid-solid mixing or mixing of bulk solids with small quantity of liquid.
- A compaction of the powder at 300 MPa.
- Sintering the sample at 540 °C for 4 hours in argon atmosphere.

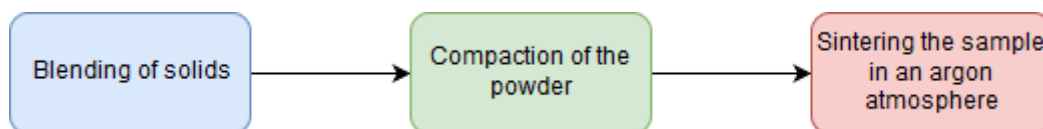


Figure 28: Block diagram of sintering AlMMC

Once we have done this, a cooling of air is necessary. Age hardening is also performed on the produced composites, carried out at a temperature of 140-170 °C for 10-14 hours.

The sintering technique used in this case is the Spark Plasma Sintering (SPS). In this process the pulsed is done by a DC that directly passes through the graphite die, as well as our powder compact and this pulse is in charge the compacting the powder. Joule heating play a dominant role in the densification of powder compacts, which results in achieving near theoretical density at lower sintering temperature compared to conventional sintering techniques. The heat generation is internal, in contrast to the conventional hot pressing, where the heat is provided by external heating elements. This facilitates a very high heating or cooling rate (up to 1000 K/min), hence the sintering process generally is very fast (within a few minutes). The general speed of the process ensures it has the potential of densifying powders with nanosize or nanostructure while avoiding coarsening which accompanies standard densification routes. This has made SPS a good method for preparation of ceramics based on nanoparticles with enhanced magnetic, magnetoelectric, piezoelectric, thermoelectric, optical or biomedical properties. SPS is the best choice for sintering the Carbon Nanotubes.

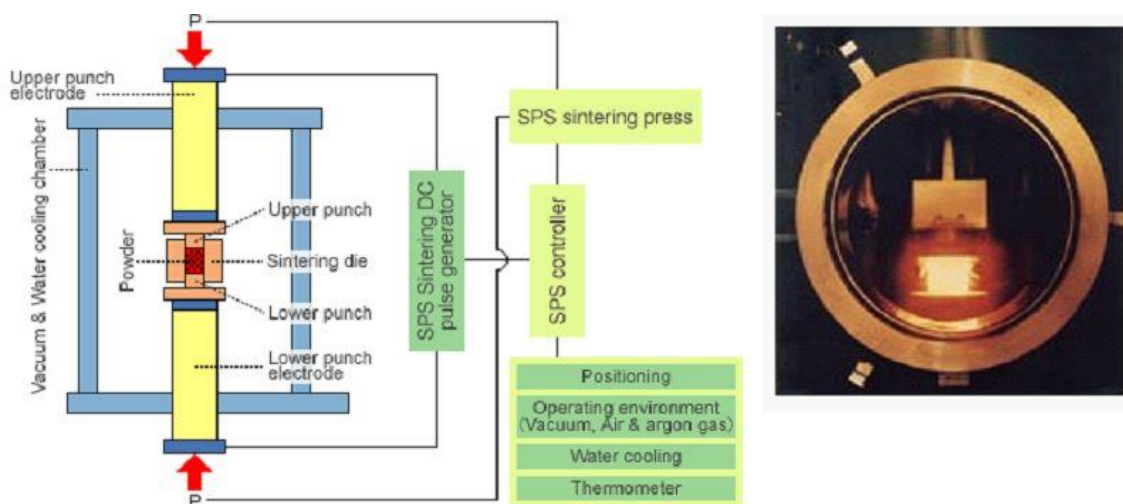


Figure 29: SPS process

In the Figure 29, can be seen the necessary equipment for this process:

- Vacuum and water cooling chamber
- Upper and lower punch electrode
- Upper and lower punch
- DC pulse generator
- Sintering press
- SPS controller

In this case we have to take into account that the used environment is argon and air.

This process also has the following characteristics:

- Generation of a local electric discharge plasma and its effect on the material.
- The combined effect of external fields, such as a force field and electric field, on densification and phase formation in a particulate system.

- The influence of electric current in the near-surface layers of conductors and semiconductors (the so-called skin effect).
- Rapid and non-uniform heating and cooling throughout the sample, causing large temperature gradients.

The basic phenomena occurring during sintering under the driving force of sintering is explain with the Figure 30.

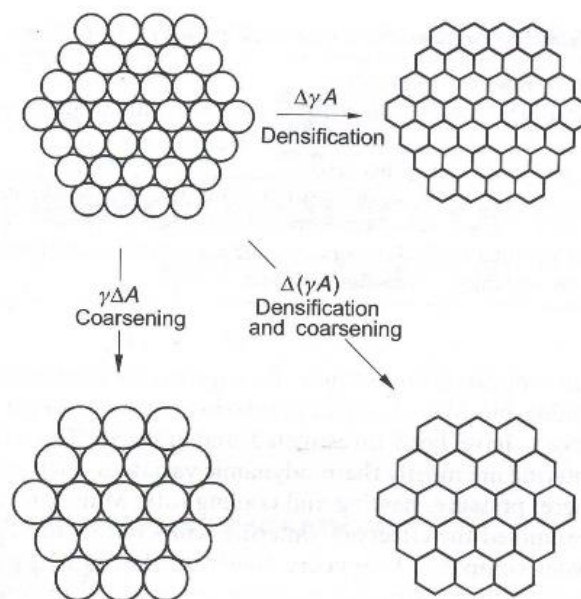


Figure 30: Sintering phenomena

The applied heat leads to a swelling effects, where the diameter of the sample is increase. In addition, fine drops of molten metal are produced on the surface of the samples due to the formation of small amounts of the super solidus liquid phase from the basic metal alloy matrix. The result of sintered co-metallized AIMMC with aluminium powder is shown in the Figure 31.



Figure 31: Sintered co-metallized AIMMC with aluminium powder

The sintering material is a matrix of an aluminium alloy turnings of 8% and up to 18% by weight of a reinforcing / un-reinforcing phase. Before the cold compaction, about 1% lubricant Zn stearate is added to the metallized mixture and homogenized by an intensive agitation. No lubricant is added to the CNTs sintering mixtures, because they themselves act as a lubricant.

The sintered co-metallized AIMMC with silicon carbide can be seen in Figure 32.



Figure 32: sintered co-metallized AIMMC with silicon carbide

The sintered co-metallized AIMMC with CNTs is shown in Figure 33.



Figure 33: sintered co-metallized AIMMC with CNTs

Dimensions of the sample

The samples for wear resistance and hardness testing are rings with an inside diameter of 23 mm, an outer diameter of 42 mm and a height of 10 mm. Due to the high reinforcing / un-reinforcing components strength, the sintered composites have a different colour and different densities.

Tests procedure

On the one hand, in order to measure the hardness of the samples a Brinell Hardness test is done. Due to the difference in densities this test is conducted according to ISO 6506-1, where it said that two load types 24.52 N and 49.03 N have to be applied at a 1 mm diameter steel ball on the Zwick 4350, Germany.

On the other hand, in order to do the tribological test, the tribometer with a “disc-roll” contact geometry is used, as shows the scheme of Figure 34.

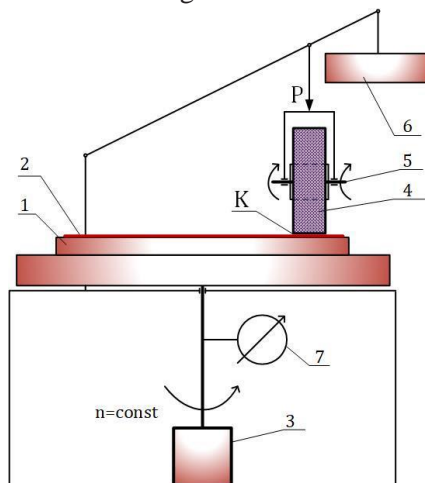


Figure 34: tribometer with a “disc-roll” contact geometry

The test specimen 4 forms a contact (K) with an abrasive surface 2, which is disposed on a horizontal disk 1. The disc 1 rotates around its central vertical axis with a constant frequency n , which is supplied by an electric motor 3. The number of revolutions (N) is measured by cyclometer 7.

The test specimen 4 is a disc that rotates freely about a horizontal axis 5. The axes of rotation of the disk 1 and of the sample 4 are two cross axes. An abrasive wear on the cylindrical surface of the specimen occurs in the contact surface (K). The contact load (P) is provided by weight 6 on the axis 5. The test specimen 4 has the following dimensions: outer diameter \varnothing 43 mm inside diameter \varnothing 23.5 mm and contact width 10 mm. The nominal contact area between the abrasive surface and the sample is about 10 mm². The linear sliding speed of the centre of gravity of the contact surface is 0.239 m/s.

Abrasive wear is calculated as a mass loss, i.e. as a difference between the initial mass of the sample and its mass after given number of abrasion cycles (N), counted by the cyclometer. Before and after testing, the mass of co-metallized AIMMC disc is measured by the electronic balance with accuracy of 0.1 mg. Normal contact load of 250 g (2.45 N) is constant for all tests and co-metallized AIMMC. The sliding distance (S) is calculated from the following equation:

$$(1) S = 2\pi N r$$

where: $r = 35$ mm is the distance between the rotational axis of disc sample and mass centre of the contact area, and N is the number of abrasion cycles.

The wear resistance I is calculated according to the formula:

$$(2) I = \rho A_a S / m$$

where:

ρ - the density of the composite material

Aa - the nominal contact surface

m - the measured mass wear.

RESULTS

Once the three tests are done, three answers are obtained: the result's morphology and structure, hardness and tribology.

Morphology and Structure of the AlMMC Composites

Firstly, in this part a SEM (x3000) is carry out to the sintered co-metallized AlMMC with 18% by weight of aluminium powder. The photos show globalized during the sintering aluminium powder (with a melting point of 660 °C) between regions with a locally crystallized super solidus liquid phase, as it is shown in Figure 35.

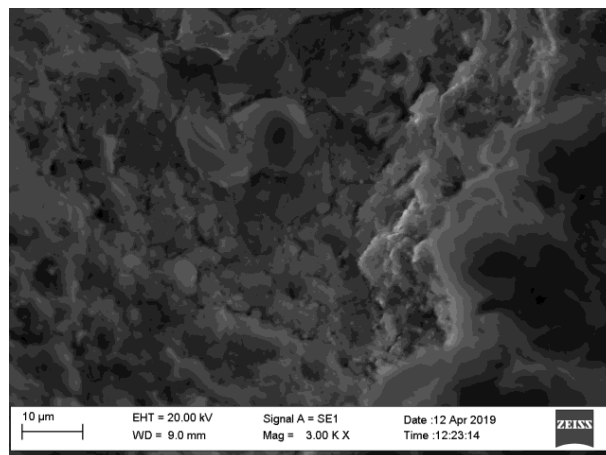


Figure 35: SEM of sintered co-metallized AlMMC with aluminium powder

Then, the EDX microanalysis, that is, the mapping and the spectrum, show the presence of the elements Ni and Cu, which prove the committed nickel-copper coating, and can be seen in Figure 36 and 37.

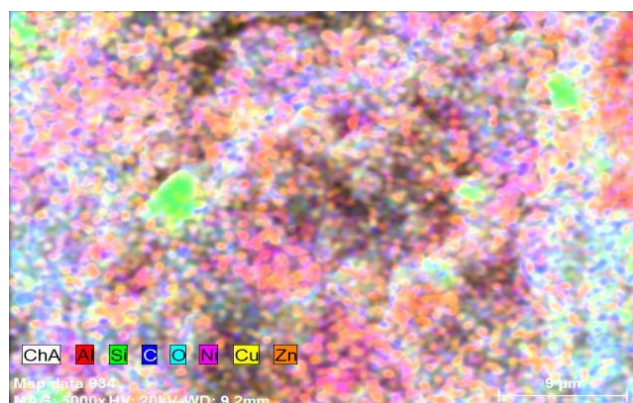


Figure 36: EDX mapping of sintered co-metallized AlMMC with aluminium powder

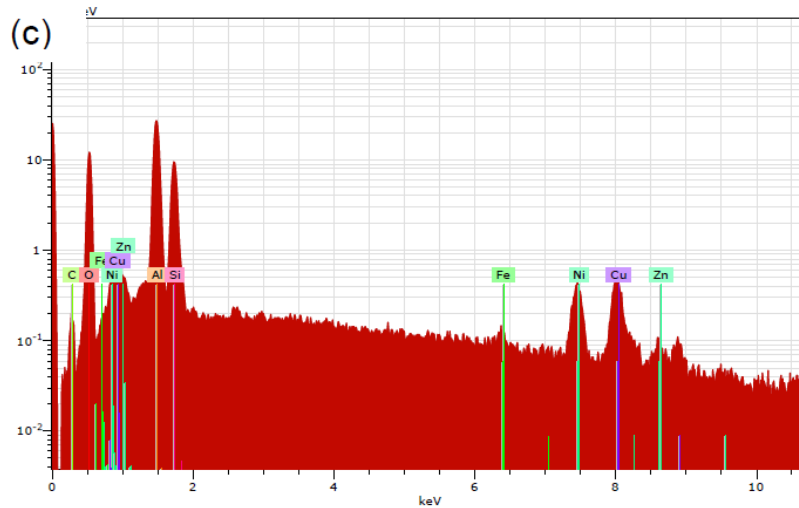


Figure 37: EDX spectrum of sintered co-metallized AlMMC with aluminium powder

Then, the same will be done to sintered co-metallized AlMMC with 18 % silicon carbide and aluminium powder in a ratio of (1:1). In this first photo can be seen the silicon carbide particles with their typical sharp edges located in the aluminium alloy matrix, as shown in the Figure 38.

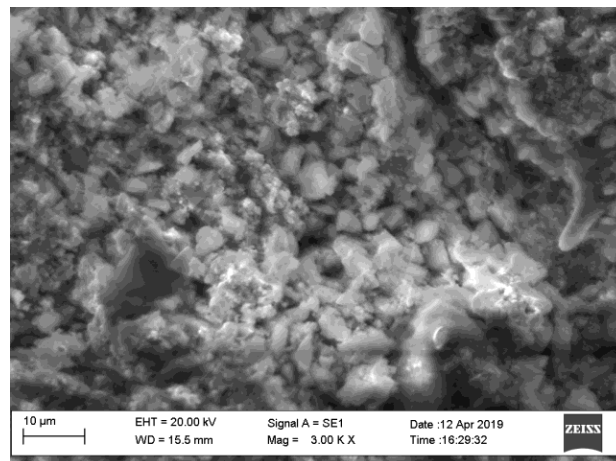


Figure 38: SEM of sintered co-metallized AlMMC with silicon carbide

The EDX microanalysis shows the presence of the elements Ni and Cu, which prove the committed nickel-copper coating, as can be seen in Figure 39 and 40.

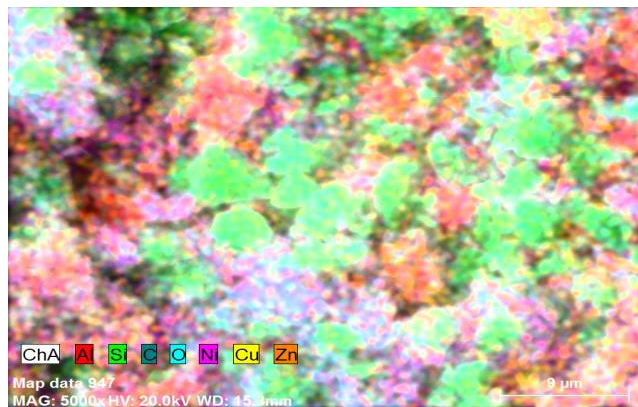


Figure 39: EDX mapping of sintered co-metallized AlMMC with silicon carbide

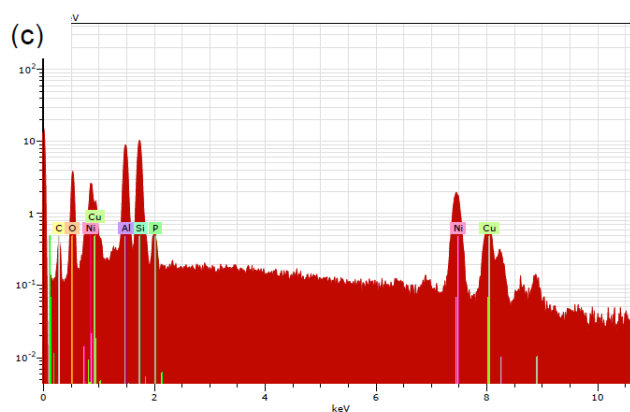


Figure 40: EDX spectrum of sintered co-metallized AlMMC with silicon carbide

Finally, the results from Scanning Electron Microscopy of fracture of sintered co-metallized AlMMC with 8 % carbon nanotubes are shown. The metallized carbon nanotubes in the aluminium matrix can be distinguished only at large magnitudes from 30 000 to 50 000 times. Distinct CNTs can be distinguished in the cluster beads formed shown in the following figure. Those clusters are seen as separate balls with a scratchy surface at smaller magnitude. The SEM with an magnification of 30 000, shown in Figure 41.

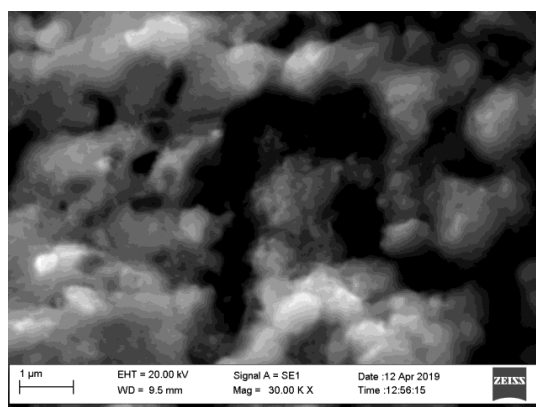


Figure 41: SEM (x30 000) of sintered co-metallized AlMMC with carbon nanotubes

The SEM with a lower magnification than the previous one can be seen in Figure 42.

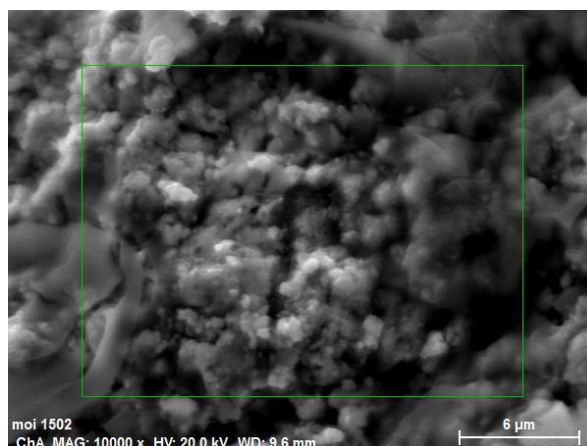


Figure 42: SEM (x10 000) of sintered co-metallized AlMMC with carbon nanotubes

And finally, the mapping is shown in Figure 43.

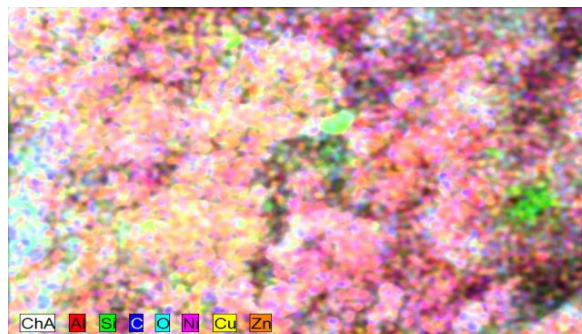


Figure 43: EDX mapping of sintered co-metallized AlMMC with carbon nanotubes

Hardness of the AlMM Composites

The hardness test has been done for sintered co-metallized AlMMC composites with different type and quantity of neutral, reinforced and un-reinforced components:

- Sample N°1: Al turnings str. acid
- Sample N°1a: Al turnings Zn str.
- Sample N°2: Al turnings Ni-Cu
- Sample N°3: Al turnings Ni-Cu+ 4g of powder
- Sample N°4: Al turnings Ni-Cu+ 4g of powder (repetition)
- Sample N°5: Al turnings Ni-Cu + 2g of SiC
- Sample N°6: Al turnings Ni-Cu + 4g of SiC
- Sample N°7/8: Al turnings clear + CNTs 1:1
- Sample N°9: Al turnings + CNTs 2:1

Before filling the tables is necessary how to calculate the deviation and the standard deviation. The deviation as it is seen in the tables is the square of the difference between the measured Brinell hardness and the average value of the hardness.

In order to calculate the standard deviation, it is used the formula shown in the EN ISO 06506-1-2014:

$$(3) s_H = \sqrt{\frac{1}{n-1} \sum_{i=1}^n (H_i - \bar{H})^2}$$

where

$\sum_{i=1}^n (H_i - \bar{H})^2$: average value of Brinell hardness

s_H : standard deviation

n : number of measurement

In the Tables from 6 to 16 show the standard values of the Brinell hardness, catch from the EN ISO 06506-4-2014, its average value and the corresponding standard deviation.

Sample N°1

The temperature and the applied load are respectively, 560 °C and a load of 2.5 kgf.

In order	1st diameter	2nd diameter	Medium value, μm	HBS	Deviation $(NB_i - HB_{\text{avg}})^2$	MAX	MIN
1	8	9	425	16,8	3,74	3,07	-1,93
2	8,2	8	405	18,6	0,02		
3	8,5	8,5	425	16,8	3,74		
4	7,5	9	413	17,8	0,87		
5	8	8	400	19,1	0,13		
6	7,5	8,4	398	19,3	0,32		
7	7,3	7,7	375	21,8	9,40		
8	7,5	8,2	393	19,8	1,14		
9	8	8,2	405	18,6	0,02		
Average				18,7	2,15	21,80	16,80
Standard deviation					0,52		

Table 6

Sample N°1a

The temperature and the applied load are respectively, 540 °C and a load of 2.5 kgf.

In order	1st diameter	2nd diameter	Medium value, μm	HBS	Deviation $(NB_i - HB_{\text{avg}})^2$	MAX	MIN
1	6,8	7	345	25,9	0,15	2,39	-3,11
2	7	7	350	25,2	0,10		
3	7	6,6	340	26,7	1,41		
4	7	7,8	370	22,4	9,68		
5	7,2	7,2	360	23,7	3,28		
6	6,8	6,8	340	26,7	1,41		
7	7	6,8	345	25,9	0,15		
8	7	6,3	333	27,9	5,71		
9	7	7	350	25,2	0,10		
Average				25,5	2,44	27,90	22,40
Standard deviation					0,55		

Table 7

Sample N°2

The temperature and the applied load are respectively, 540 °C and a load of 2.5 kgf.

In order	1st diameter	2nd diameter	Medium value, μm	HBS	Deviation $(NB_i - HB_{avg})^2$	MAX	MIN
1	6,4	7	335	27,5	10,24	3,90	-4,80
2	6	6	300	34,6	15,21		
3	6,3	5,8	303	33,9	10,24		
4	6	6	300	34,6	15,21		
5	6	7	325	29,3	1,96		
6	6	6	300	34,6	15,21		
7	7	6,8	345	25,9	23,04		
8	7	6,4	335	27,5	10,24		
9	6,6	6,6	330	28,4	5,29		
Average				30,7	11,8	34,60	25,90
Standard deviation					1,22		

Table 8

Sample N°3

The temperature and the applied load are respectively, 540 °C and a load of 5 kgf.

In order	1st diameter	2nd diameter	Medium value, μm	HBS	Deviation $(NB_i - HB_{avg})^2$	MAX	MIN
1	7	8	375	43,6	7,4	3,99	-5,01
2	7	7	350	50,3	15,9		
3	7,4	7,4	370	44,9	2,0		
4	7	7	350	50,3	15,9		
5	7	7	350	50,3	15,9		
6	7	8	375	43,6	7,4		
7	7	7,2	355	48,9	6,7		
8	7,4	8	385	41,3	25,1		
9	7	8	375	43,6	7,4		
Average				46,3	11,5	50,30	41,30
Standard deviation					1,20		

Table 9

Sample N°4

The temperature and the applied load are respectively, 540 °C and a load of 5 kgf.

In order	1st diameter	2nd diameter	Medium value, μm	HBS	Deviation $(\text{NB}_i - \text{HB}_{\text{avg}})^2$	MAX	MIN
1	7	7,4	360	47,5	14,95	3,87	-4,53
2	7	7,4	360	47,5	14,95		
3	7,3	7,5	370	44,9	1,60		
4	7,4	7,4	370	44,9	1,60		
5	8	7,6	390	40,2	11,79		
6	8	7,4	385	41,3	5,44		
7	7,6	7,2	370	44,9	1,60		
8	8	7,8	395	39,1	20,55		
9	7,4	7,8	380	42,4	1,52		
Average				43,6	8,2	47,50	39,10
Standard deviation					1,01		

Table 10

Sample N°5

The temperature and the applied load are respectively, 540 °C and a load of 5 kgf.

In order	1st diameter	2nd diameter	Medium value, μm	HBS	Deviation $(\text{NB}_i - \text{HB}_{\text{avg}})^2$	MAX	MIN
1	6,3	6,4	318	61,3	31,36	5,60	-3,90
2	6,3	7	333	55,8	0,01		
3	6,8	6,6	335	55,1	0,36		
4	6,8	6,4	330	56,8	1,21		
5	6	7	325	58,6	8,41		
6	7	6,8	345	51,8	15,21		
7	7	6,4	335	55,1	0,36		
8	6,8	6,8	340	53,4	5,29		
9	6,6	7	340	53,4	5,29		
Average				55,7	7,5	61,30	51,80
Standard deviation					0,97		

Table 11

Sample N°6

The temperature and the applied load are respectively, 540 °C and a load of 5 kgf.

In order	1st diameter	2nd diameter	Medium value, μm	HBS	Deviation $(\text{NB}_i - \text{HB}_{\text{avg}})^2$	MAX	MIN
1	7	6,4	335	55,1	17,08	4,13	-3,47
2	7,3	7	358	48,0	8,80		
3	6,8	7	345	51,8	0,69		
4	7	7	350	50,3	0,44		
5	7	7	350	50,3	0,44		
6	6,4	7	335	55,1	17,08		
7	7	7	350	50,3	0,44		
8	7	7,4	360	47,5	12,02		
9	7	7	350	50,3	0,44		
Average				51,0	6,4	55,10	47,50
Standard deviation					0,89		

Table 12

Sample N°7/8

The temperature and the applied load are respectively, 540 °C and a load of 1 kgf.

In order	1st diameter	2nd diameter	Medium value, μm	HBS	Deviation $(\text{NB}_i - \text{HB}_{\text{avg}})^2$	MAX	MIN
1	7	7,4	360	9,5	1,93	2,91	-1,39
2	6,6	6	315	12,5	2,60		
3	7	7	350	10,1	0,62		
4	7,4	7	360	9,5	1,93		
5	7	7	350	10,1	0,62		
6	7	7	350	10,1	0,62		
7	6	6	300	13,8	8,47		
8	7	6,4	335	11,0	0,01		
9	6,4	6,8	330	11,4	0,26		
Average				10,9	1,9	13,80	9,50
Standard deviation					0,49		

Table 13

Sample N°9

The temperature and the applied load are respectively, 540 °C and a load of 2.5 kgf.

In order	1st diameter	2nd diameter	Medium value, μm	HBS	Deviation $(NB_i - HB_{avg})^2$	MAX	MIN
1	7,8	8	395	19,6	2,81	2,18	-3,02
2	8	8,4	410	18,1	0,03		
3	9	9	450	14,9	9,13		
4	8	8	400	19,1	1,39		
5	9	9	450	14,9	9,13		
6	8,4	8,8	430	16,4	2,32		
7	8	8	400	19,1	1,39		
8	8	7,6	390	20,1	4,74		
9	8	8	400	19,1	1,39		
Average				17,9	3,6	20,10	14,90
Standard deviation					0,67		

Table 14

Sample N°10

The temperature and the applied load are respectively, 540 °C and a load of 2.5 kgf.

In order	1st diameter	2nd diameter	Medium value, μm	HBS	Deviation $(NB_i - HB_{avg})^2$	MAX	MIN
1	7,6	7	365	23,1	5,76	4,50	-3,10
2	7	8	375	21,8	1,21		
3	7	7,4	360	23,7	9,00		
4	8	8	400	19,1	2,56		
5	8	8	400	19,1	2,56		
6	7	7	350	25,2	20,25		
7	8,4	8,2	415	17,6	9,61		
8	8	8	400	19,1	2,56		
9	8,6	8	415	17,6	9,61		
Average				20,7	7,0	25,20	17,60
Standard deviation					0,94		

Table 15

Sample N°13

The temperature and the applied load are respectively, 540 °C and a load of 2.5 kgf.

In order	1st diameter	2nd diameter	Medium value, μm	HBS	Deviation $(NB_i - HB_{avg})^2$	MAX	MIN
1	8,3	9	433	16,1	3,91		
2	8	7,2	380	21,2	9,75		
3	7	8	375	21,8	13,85		
4	8,6	9	440	15,6	6,14		
5	7	7,4	360	23,7	31,61	5,62	-3,18
6	8,4	8	410	18,1	0,00		
7	9	9	450	14,9	10,10		
8	8,4	8,8	430	16,4	2,81		
9	9	9	450	14,9	10,10		
Average				18,1	9,8	23,70	14,90
Standard deviation					1,11		

Table 16

A graph has been built with the average value of the Brinell hardness, this is shown in Figure 44.

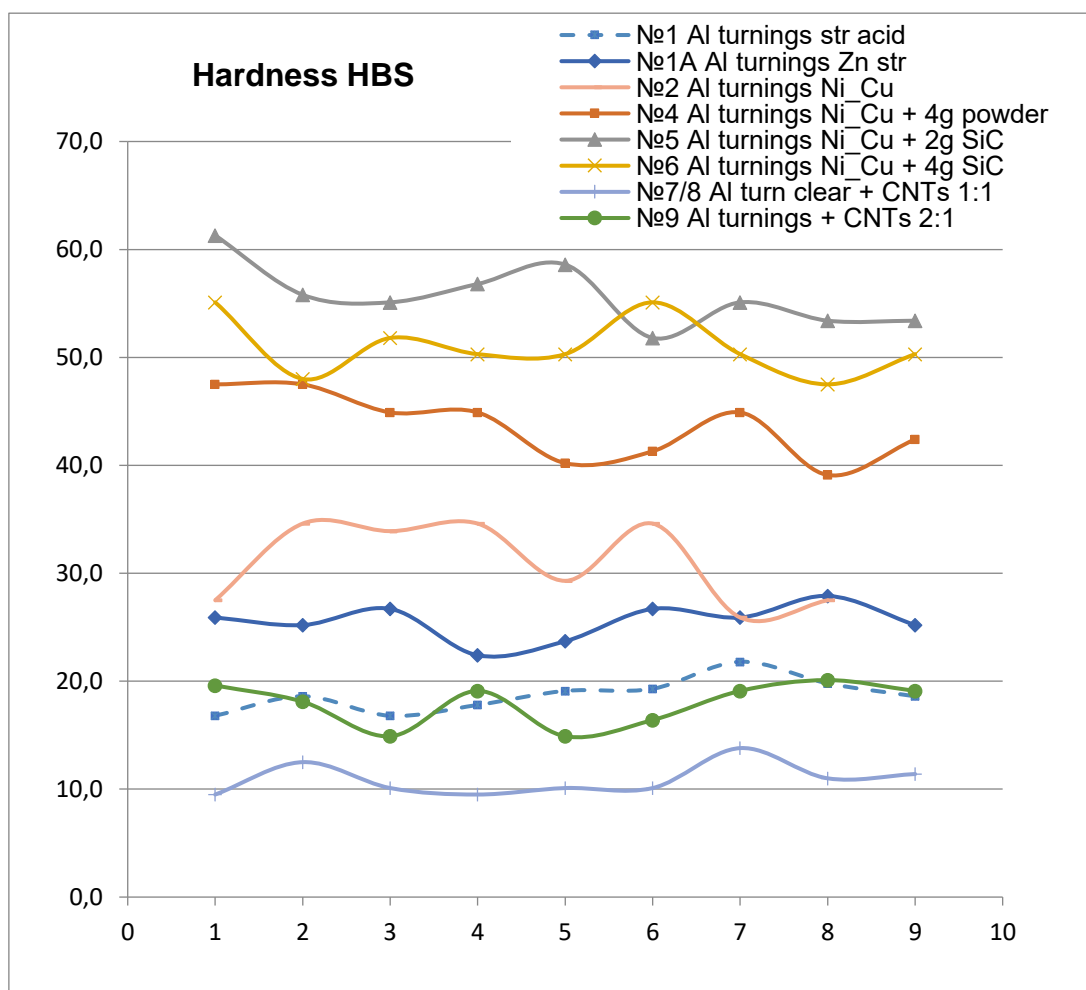


Figure 44: Average values of Brinell Hardness of each sample

So in order to summarize, the following table is built, where the hardness (mean value and standard deviation) is related with the density of the samples, and this can be seen in Table 17.

Sintered sample	Density (g/cm ³)	HBS	
		Mean value	s _H
N°1a	1.76	25.5	0.55
N°2	2.29	30.7	1.22
N°3	2.5	46.3	1.20
N°4	2.54	43.6	1.01
N°5	2.22	55.7	0.97
N°6	2.26	51.0	0.89
N°7/8	1.77	10.9	0.49
N°10	1.87	20.7	0.94
N°13	1.78	18.1	1.11

Table 17: Relation between density and hardness of the samples

The density and the hardness of sintered co-metallized AIMM composites depends on the type and the percentage of the metallised dispersed phase, as we have seen in the Table 17. The Ni-Cu coating of aluminium turnings leads to a 20% increase in the hardness, but also to an increase in the non-uniformity of the composite structure.

Inserting the neutral aluminium powder to the aluminium turnings increases the hardness with 70-80% and improves the interfacial bonding in the sintered composite.

Highest hardness values have related to ceramic reinforcement composites (silicon carbide and aluminium powder SiC and Al powder) in which a double increase was observed. The excessive increase in the percentage of the reinforcement phase from 8 % to 18 % leads not only to a slight decrease in the hardness and the density, but also to a degradation of the turnings' interfacial bonding into the common aluminium alloy matrix.

Lowest values of the mechanical parameters and the density is accounted in the sintered co-metallized AIMMC with CNTs. Their comparison with other composites and their behaviour during the wear resistance and hardness test shows that the CNTs to a large extent preserved their original structure in the aluminium alloy matrix and they did not break into soot during the compaction at 300 MPa.

The evaluation of this behaviour, determination of their friction coefficient and finding more suitable sintering modes are a subject to future research on improving the mechanical behaviour of those AIMMC.

Tribological properties of the AIMM Composites

Firstly, the results from the determination of the mass wear rate and wear resistance of sintered co-metallized AIMM Composites with neutral and reinforcing components are shown. Here we have the following samples:

- Sample N°1: Al turnings only at 560 °C
- Sample N°1a: Al turnings only (reference)
- Sample N°2: Al turnings all metalized Ni-Cu
- Sample N°3: Al turnings + 8% powder all Ni-Cu
- Sample N°4: Al turnings + 18% powder all Ni-Cu

- Sample N°5: Al turnings + 8% SiC all Ni-Cu
- Sample N°6: Al turnings + 18% SiC all Ni-Cu

As have been done with the hardness, the tables from 18 to 24 will be build, taking into account the formulas shown in the tables.

Sample N°1a

Cycle number	Sample mass, t	Friction path, L	Wearing, m	Wear speed, γ	Wear intensity $i = m/\rho \cdot L \cdot Aa$	Wear resistance $I = \rho \cdot L \cdot Aa/m \cdot 10^{-4}$
N	g	m	mg	mg/m	-	-
0	19,3938	0,00	0,000	0,0000	0,00	0
100	19,2831	21,98	0,111	0,0050	2,64E-07	378
200	19,1819	43,96	0,212	0,0048	2,53E-07	395
300	19,1051	65,94	0,289	0,0044	2,30E-07	435
400	18,9470	87,92	0,447	0,0051	2,67E-07	375
Wear	0,4468				Average	402

Table 18

Sample N°1

Cycle number	Sample mass, t	Friction path, L	Wearing, m	Wear speed, γ	Wear intensity $i = m/\rho \cdot L \cdot Aa$	Wear resistance $I = \rho \cdot L \cdot Aa/m \cdot 10^{-4}$
N	g	m	mg	mg/m	-	-
0	17,9590	0,00	0,000	0,0000	0,00	0
100	17,8335	21,98	0,125	0,0057	3,24E-07	309
200	17,7357	43,96	0,223	0,0051	2,88E-07	347
300	17,6672	65,94	0,292	0,0044	2,51E-07	399
400	17,6155	87,92	0,343	0,0039	2,21E-07	452
Wear	0,3435				Average	399

Table 19

In the following samples the relative wear resistance is also calculated:

Sample N°2

Cycle number	Sample mass, t	Friction path, L	Wearing, m	Wear speed, γ	Wear intensity $i = m/\rho \cdot L \cdot Aa$	Wear resistance $I = \rho \cdot L \cdot Aa/m \cdot 10^{-4}$	Relative wear resistance.
N	g	m	mg	mg/m	-	-	%
0	23,3048	0,00	0,000	0,0000	0,00	0	
100	23,0157	21,98	0,289	0,0132	5,75E-07	174	-43,7
200	22,7798	43,96	0,525	0,0119	5,22E-07	192	-44,8
300	22,6010	65,94	0,704	0,0107	4,66E-07	214	-46,2
400	22,4739	87,92	0,831	0,0095	4,13E-07	242	-46,4
Wear	0,8309				Average	216	-45,3

Table 20

Sample N°3

Cycle number	Sample mass, t	Friction path, L	Wearing, m	Wear speed, γ	Wear intensity $i = m/\rho \cdot L \cdot Aa$	Wear resistance $I = \rho \cdot L \cdot Aa/m \cdot 10^{-4}$	Relative wear resistance.
N	g	m	mg	mg/m	-	-	%
0	25,4954	0,00	0,000	0,0000	0,00	0	
100	25,4038	21,98	0,092	0,0042	1,66E-07	601	94,5
200	25,3475	43,96	0,148	0,0034	1,34E-07	744	114,3
300	25,3035	65,94	0,192	0,0029	1,16E-07	861	115,9
400	25,2684	87,92	0,227	0,0026	1,03E-07	970	114,8
Wear	0,2270				Average	858	109,9

Table 21

Sample N°4

Cycle number	Sample mass, t	Friction path, L	Wearing, m	Wear speed, γ	Wear intensity $i = m/\rho \cdot L \cdot Aa$	Wear resistance $I = \rho \cdot L \cdot Aa/m \cdot 10^{-4}$	Relative wear resistance.
N	g	m	mg	mg/m	-	-	%
0	25,8692	0,00	0,000	0,0000	0,00	0	
100	25,7680	21,98	0,101	0,0046	1,81E-07	552	78,6
200	25,6932	43,96	0,176	0,0040	1,58E-07	635	82,8
300	25,6273	65,94	0,242	0,0037	1,44E-07	693	73,8
400	25,5885	87,92	0,281	0,0032	1,26E-07	796	76,3
Wear	0,2807				Average	708	77,9

Table 22

Sample N°5

Cycle number	Sample mass, t	Friction path, L	Wearing, m	Wear speed, γ	Wear intensity $i = m/\rho \cdot L \cdot Aa$	Wear resistance $I = \rho \cdot L \cdot Aa/m \cdot 10^{-4}$	Relative wear resistance.
N	g	m	mg	mg/m	-	-	%
0	22,6163	0,00	0,000	0,0000	0,00	0	
100	22,4907	21,98	0,126	0,0057	2,57E-07	389	25,8
200	22,4114	43,96	0,205	0,0047	2,10E-07	477	37,2
300	22,3421	65,94	0,274	0,0042	1,87E-07	534	34,0
400	22,2837	87,92	0,333	0,0038	1,70E-07	587	30,1
Wear	0,3326				Average	533	31,8

Table 23

Sample N°6

Cycle number	Sample mass, t	Friction path, L	Wearing, m	Wear speed, γ	Wear intensity $i = m/\rho \cdot L \cdot Aa$	Wear resistance $I = \rho \cdot L \cdot Aa/m \cdot 10^{-4}$	Relative wear resistance.
N	g	m	mg	mg/m	-	-	%
0	23,0403	0,00	0,000	0,0000	0,00	0	
100	22,9187	21,98	0,122	0,0055	2,44E-07	409	32,5
200	22,8444	43,96	0,196	0,0045	1,97E-07	508	46,3
300	22,7809	65,94	0,259	0,0039	1,74E-07	575	44,3
400	22,7273	87,92	0,313	0,0036	1,57E-07	636	40,8
Wear	0,3130				Average	573	41,0

Table 24

Once, the previous tables are filled, we will build the three different graphs: a graph with the wear rate (Figure 45), another one with the wear resistance (Figure 46) and finally another one with the relative wear resistance (Figure 47).

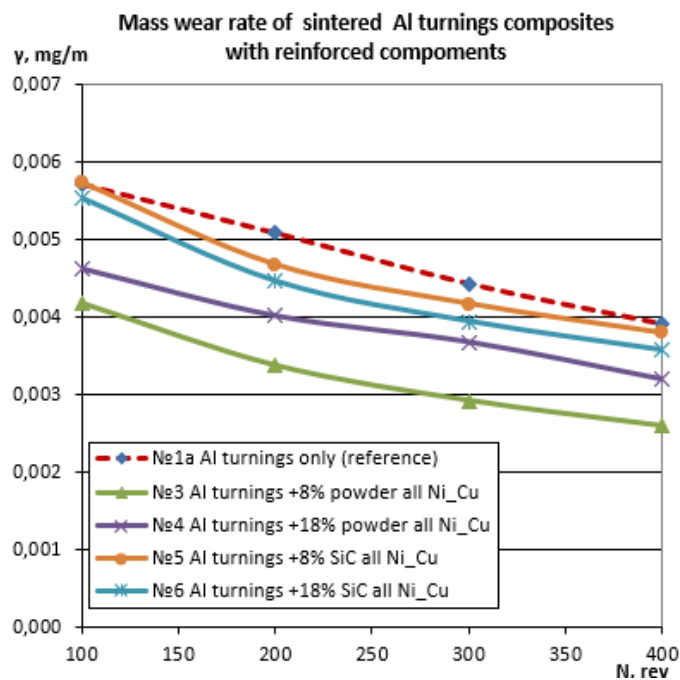


Figure 45: Mass wear rate of sintered co-metallized AlMM Composites with neutral and reinforcing components

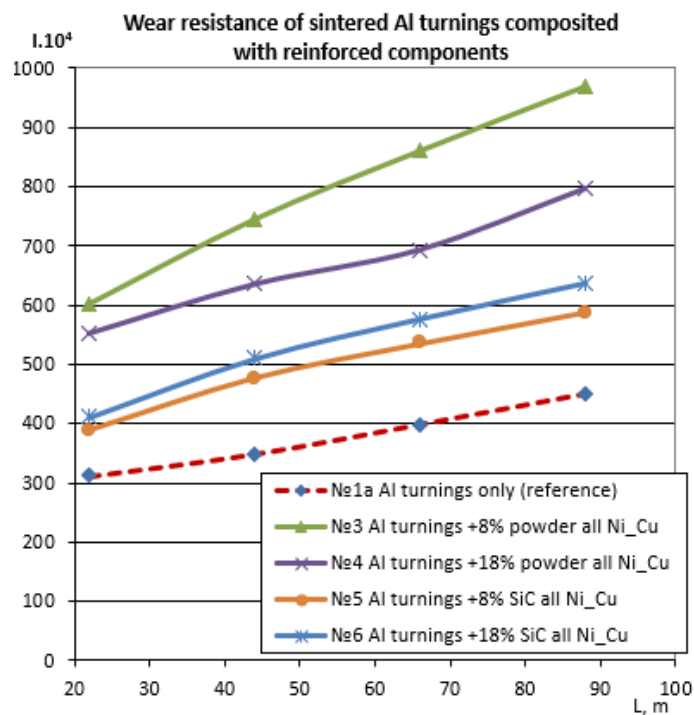


Figure 46: Wear resistance of sintered co-metallized AlMM Composites with neutral and reinforcing components

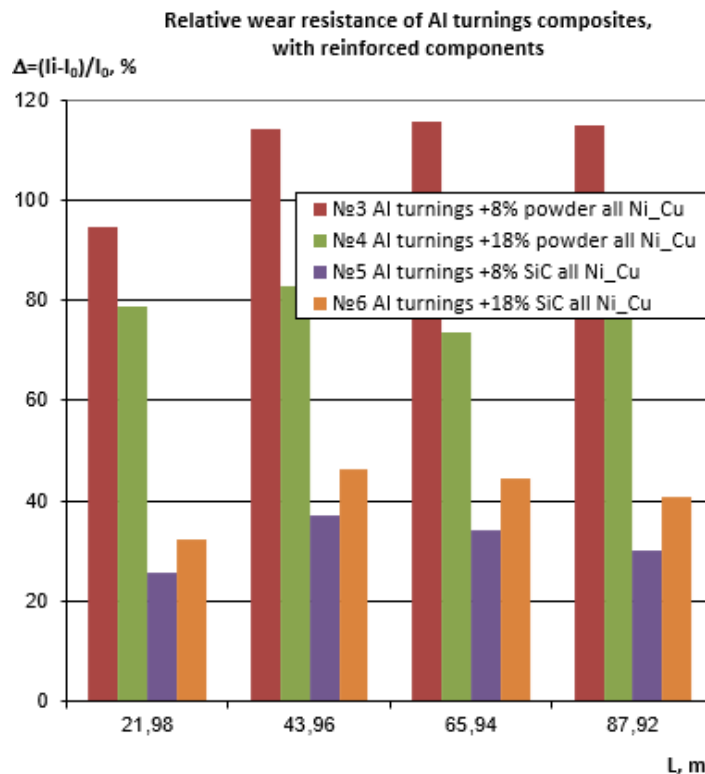


Figure 47: Relative wear resistance of sintered co-metallized AIMM Composites with neutral and reinforcing components

The Figures 45 and 46 shows that on the one hand, the Al turning without any additional components has the highest wear rate and the lowest wear resistance, as expected. On the other hand, the sintered co-metallized AIMMC with 8 % Al powder has the lowest wear rate and the highest wear resistance. Besides, can be seen that the wear resistance in the sintered co-metallized AIMMC with 8 % Al powder has almost increased like 50%.

On the previous Figure 47, the sintered co-metallized AIMM composites are compared to the reference sample in regard to their relative abrasion wear resistance. There can be seen how the sintered co-metallized AIMMC with 8 % Al powder has an increase of 100-120 % in the wear resistance while the sintered co-metallized AIMMC with 8 % of SiC has the lowest increase with percentage between 20-40 %.

Then, the results from the determination of the mass wear rate and wear resistance of sintered co-metallized AIMM Composites with reinforcing components and CNTs are shown. Here we have the following samples:

- Sample N°1: Al turnings only at 560 °C
- Sample N°1a: Al turnings only (reference)
- Sample N°2: Al turnings all metalized Ni-Cu
- Sample N°10: Al turnings + 4% CNTs all Ni-Cu
- Sample N°8: Al turnings + 8% CNTs all Ni-Cu
- Sample N°13: only 8% CNTs all Ni-Cu

With this samples Tables from 25 to 30 will be filled.

Sample N°1

Cycle number	Sample mass, t	Friction path, L	Wearing m	Wear speed, γ	Wear intensity $i = m/\rho \cdot L \cdot Aa$	Wear resistance $I = \rho \cdot L \cdot Aa/m \cdot 10^{-4}$
N	g	m	mg	mg/m	-	-
0	19,3938	0,00	0,000	0,0000	0,00	0
100	19,2831	21,98	0,111	0,0050	2,64E-07	378
200	19,1819	43,96	0,212	0,0048	2,53E-07	395
300	19,1051	65,94	0,289	0,0044	2,30E-07	435
400	18,9470	87,92	0,447	0,0051	2,67E-07	375
Wear	0,4468				Average	402

Table 25

Sample N°1a

Cycle number	Sample mass, t	Friction path, L	Wearing m	Wear speed, γ	Wear intensity $i = m/\rho \cdot L \cdot Aa$	Wear resistance $I = \rho \cdot L \cdot Aa/m \cdot 10^{-4}$
N	g	m	mg	mg/m	-	-
0	17,9590	0,00	0,000	0,0000	0,00	0
100	17,8335	21,98	0,125	0,0057	3,24E-07	309
200	17,7357	43,96	0,223	0,0051	2,88E-07	347
300	17,6672	65,94	0,292	0,0044	2,51E-07	399
400	17,6155	87,92	0,343	0,0039	2,21E-07	452
Wear	0,3435				Average	399

Table 26

In the following samples the relative wear resistance is also calculated:

Sample N°2

Cycle number	Sample mass, t	Friction path, L	Wearing m	Wear speed, γ	Wear intensity $i = m/\rho \cdot L \cdot Aa$	Wear resistance $I = \rho \cdot L \cdot Aa/m \cdot 10^{-4}$	Relative wear resistance.
N	g	m	mg	mg/m	-	-	%
0	23,3048	0,00	0,000	0,0000	0,00	0	
100	23,0157	21,98	0,289	0,0132	5,75E-07	174	-43,7
200	22,7798	43,96	0,525	0,0119	5,22E-07	192	-44,8
300	22,6010	65,94	0,704	0,0107	4,66E-07	214	-46,2
400	22,4739	87,92	0,831	0,0095	4,13E-07	242	-46,4
Wear	0,8309				Average	216	-45,3

Table 27

Sample N°10

Cycle number	Sample mass, t	Friction path, L	Wearing m	Wear speed γ	Wear intensity $i = m/\rho \cdot L \cdot Aa$	Wear resistance $I = \rho \cdot L \cdot Aa/m \cdot 10^{-4}$	Relative wear resistance.
N	g	m	mg	mg/m	-	-	%
0	19,0075	0,00	0,000	0,0000	0,00	0	
100	18,7954	21,98	0,212	0,0096	5,17E-07	194	-37,4
200	18,5883	43,96	0,419	0,0095	5,11E-07	196	-43,6
300	18,4048	65,94	0,603	0,0091	4,90E-07	204	-48,8
400	18,2407	87,92	0,767	0,0087	4,67E-07	214	-52,6
Wear	0,7668				Average	205	-45,6

Table 28

Sample N°8

Cycle number	Sample mass, t	Friction path, L	Wearing m	Wear speed, γ	Wear intensity $i = m/\rho \cdot L \cdot Aa$	Wear resistance $I = \rho \cdot L \cdot Aa/m \cdot 10^{-4}$	Relative wear resistance.
N	g	m	mg	mg/m	-	-	%
0	18,0635	0,00	0,000	0,0000	0,00	0	
100	17,5071	21,98	0,556	0,0253	1,43E-06	70	-77,3
200	17,1648	43,96	0,899	0,0204	1,15E-06	87	-75,0
300	16,9461	65,94	1,117	0,0169	9,55E-07	105	-73,7
400	16,7575	87,92	1,306	0,0149	8,37E-07	119	-73,5
Wear	1,3060				Average	104	-74,9

Table 29

Sample N°13

Cycle number	Sample mass, t	Friction path, L	Wearing m	Wear speed, γ	Wear intensity $i = m/\rho \cdot L \cdot Aa$	Wear resistance $I = \rho \cdot L \cdot Aa/m \cdot 10^{-4}$	Relative wear resistance.
N	g	m	mg	mg/m	-	-	%
0	18,1066	0,00	0,000	0,0000	0,00	0	
100	17,9146	21,98	0,192	0,0087	4,91E-07	204	-34,1
200	17,8557	43,96	0,251	0,0057	3,21E-07	312	-10,3
300	17,7955	65,94	0,311	0,0047	2,65E-07	377	-5,4
400	17,7341	87,92	0,372	0,0042	2,38E-07	420	-7,0
Wear	0,3725				Average	369	-14,2

Table 30

Once the previous tables are filled, we will build the same graphs as previous, which go from Figure 48 to 50.

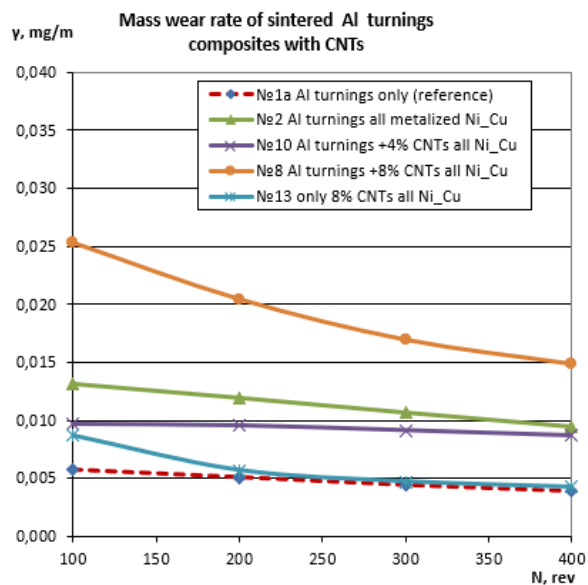


Figure 48: Mass wear rate of sintered co-metallized AIMM Composites with reinforcing components and CNTs

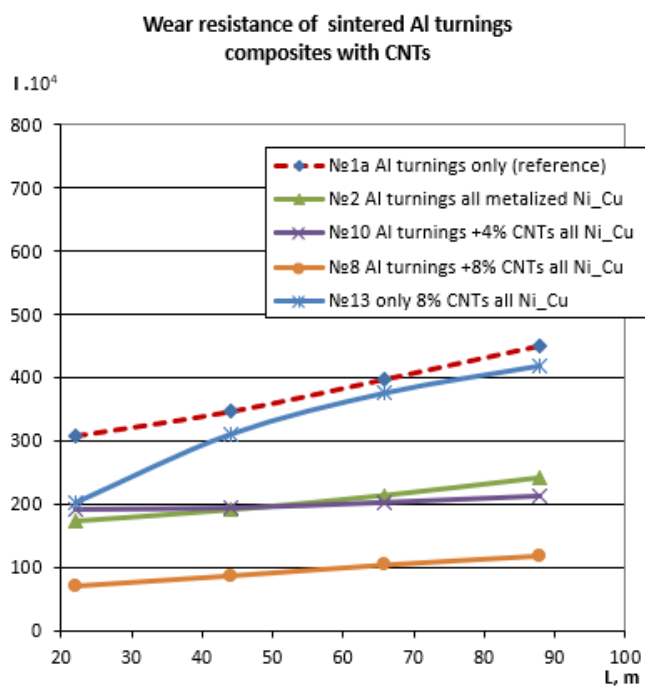


Figure 49: Wear resistance of sintered co-metallized AIMM Composites with reinforcing components and CNTs

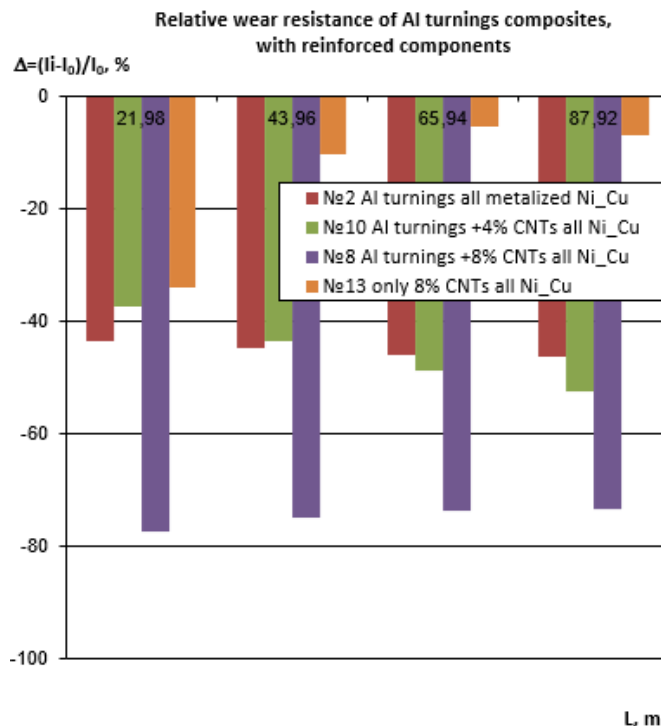


Figure 50: Relative wear resistance of sintered co-metallized AIMMC Composites with reinforcing components and CNTs

In the first two graphs can be seen that the Al turning without any additional component, unlike the previous case, has the lowest wear rate and the highest wear resistance. In this case the sintered co-metallized AIMMC un-reinforced with CNTs shows the worst behaviour having the highest wear rate and the lowest wear resistance. So this means that due to the metallization, they have retained their structure and they did not decay to soot during the compaction. However, this results in an instability of the composite material and it does not allow the integration of a higher percentage of CNTs into the aluminium alloy matrix.

The metal-metal composite of metallized (Ni-Cu) aluminium turnings without an additional phase also give a worse behaviour to the material, because it increase the wear rate and decrease the wear resistance.

The component nearer the behaviour of the Al turning without any additional component, is the Ni-Cu metallized carbon fibre CNTs without aluminium turnings. But surely it has a different coefficient of contact friction.

In the Figure 50 can be seen that all the samples make a decrease in the wear resistance if we compared to the reference sample in regard to their relative abrasion wear resistance. The one with the lowest decrease is the Ni-Cu metallized carbon fibre CNTs without aluminium turnings, and the one with the highest decrease is the sintered co-metallized AIMMC un-reinforced with 8 % of CNTs, with a decrease of moreover 75 %.

CONCLUSIONS

Once this experiment has been done, some conclusions are obtained regarding to the obtained results.

This experiment has shown how the addition of a neutral phase with another fractional composition to the aluminium turnings, which is aluminium powder, significantly improves the interfacial bonding, the hardness and the wear resistance of the sintered co-metallized AIMM composites. That makes this material a good choice to work with, for example in the automotive applications, which is the principal aim of this experiment.

The reinforcement of co-metallized ceramics, in this case SiC, in AIMMC makes this material harder, with a double increasing of hardness. But that reinforcement has a limit, so an excessive reinforcement leads to a deterioration of bonding into the common aluminium alloy matrix. Quantities of the reinforcement element has to be controlled.

The addition of CNTs to the sample shows the lowest densities and also the worst mechanical and tribological performance. Through the metallization CNTs have retained their fibrous structure after the cold compaction, this is known thanks to the tests results and the SEM pictures.

In addition, it has been proven that it is possible to sinter composite material only from electroless metallized CNTs obtained by further heating of the solution described in the work. The specimen from metallized CNTs has a wear resistance commensurate with that of the reference sample, but is likely to have a very different coefficient of contact friction.

BIBLIOGRAPHY

1. **Mehdi Rahimian, Naser Ehsani, Nader Parvin, Hamid reza Baharvandi.** “The effect of particle size, sintering temperature and sintering time on the properties of Al–Al₂O₃ composites, made by powder metallurgy”. *Journal of Materials Processing Technology*. April 2009.
2. **M. G. Ananda Kumara, S.Seetharamu, Jagannath Nayakb, L.N. Satapathyc.** “A Study on Thermal Behaviour of Aluminium Cenosphere Powder Metallurgy Composites Sintered in Microwave”. Elsevier. May 2014.
3. **S. Narayan and A. Rajeshkannan.** “Workability Behaviour of Powder Metallurgy Aluminium Composites”. *Journal of Powder Technology*. July 2014.
4. **S. C. Hanyaloglua, B. Aksakala, I.J. McColm.** “Reactive sintering of electroless nickel-plated aluminium powders”. Elsevier. April 2001.
5. **Tohru Sekino, Toshio Nakajima, Satoru Ueda, Koichi Niihara.** “Reduction and Sintering of a Nickel–Dispersed-Alumina Composite and Its Properties”. *Journal of Materials Processing Technology*. September 1997.
6. **M. Qian, G.B. Schaffer.** “Sintering of aluminium and its alloys”. University of Queensland, Australia.
7. **S. D. Kabushiki.** “European Patent Application”. European Patent Office. December 1990.
8. **G.B. Schaffer.** “Powder Processed Aluminium Alloys”. University of Queensland, Australia.
9. **Gökçe, F. Fındık.** “Mechanical and physical properties of sintered aluminium powders”. *Journal of Achievements in Materials and Manufacturing Engineering*. October 2008.
10. **Total Materia.** “Sintered Aluminium Powder (SAP)”. Taken from:
<http://www.totalmateria.com/Article76.htm>
11. **D. Kopeliovich.** “Sintered Aluminium Alloys”. Taken from:
http://www.substech.com/dokuwiki/doku.php?id=sintered_aluminum_alloys
12. **Arun K. Chattopadhyay.** “Enhanced Material Properties of Sintered Aluminium Powders”. *Advances in Powder Metallurgy and Particulate Materials*. October 2010.
13. **Nikhilesh Chawla, Yu-Lin Shen.** “Mechanical Behaviour of Particle Reinforced Metal Matrix Composites”. *Advanced Engineering Materials*. March 2001.
14. **Ramesh Singh.** “Coating for Corrosion Prevention”. *Corrosion control for Offshore Structures*. 2014.
15. **Sudagar, Jothi; Lian, Jianshe; Sha, Wei.** “Electroless nickel, alloy, composite and nano coatings - A critical review”. *Journal of alloys and Compounds*. 2013.
16. **G.S. Upadhyaya.** “Some issues in sintering science and technology”. *Materials Chemistry and Physics*. 2001.
17. **G. O'Donnell, L. Looney.** “Production of aluminium matrix composite components using conventional PM technology”. *Materials Science and Engineering*. 2001.
18. **S. Müller, Th. Schubert, F. Fiedler, R. Stein, B. Kieback, L. Deters.** “Properties of Sintered P/M Aluminium Composites”. 2011.
19. **Hansang Kwon, Mehdi Estili, Kenta Takagi, Takamichi Miyazaki, Akira Kawasaki.** “Combination of hot extrusion and spark plasma sintering for producing carbon nanotube reinforced aluminium matrix composites”. Elsevier. November 2008.
20. **M. Jayaram.** “Experimental Investigation of Aluminium Silicon Carbide Composites by Powder Metallurgy Technique”. *International Research Journal of Latest Trends in Engineering and Technology (IRJLTET)*. June 2015.
21. **C.F. Deng, D.Z. Wang, X.X. Zhang, A.B. Li.** “Processing and properties of carbon nanotubes reinforced aluminium composites”. Elsevier. August 2006.

22. **S.H.M. Anijdana, M. Sabzib, M.R. Zadehb, M. Farzamec.** “The Effect of Electroless Bath Parameters and Heat Treatment on the Properties of Ni-P and Ni-P-Cu Composite Coatings”. Material research. 2018.
23. **BS EN ISO 6506-1:2014.** European committee for standardization. Brussels. August 2018.
24. **BS EN ISO 6506-4:2014.** European committee for standardization. Brussels. August 2018.
25. **Valentin Kamburov, Rayna Dimitrova, Antonio Nikolov, Mara Kandeve, Anton Mihaylov.** “Aluminium Metal Matrix Composite Sintering with Electroless Metallized Components”. Serbian Tribology Society. May 2019.